CONTRIBUTION OF MODULUS TO THE CONTACT GUIDANCE OF ENDOTHELIAL CELLS ON MICROTEXTURED SILOXANE ELASTOMERS

By

WADE RICHARD WILKERSON

A THESIS PRESENTED TO THE GRADUATE SCHOOL
OF THE UNIVERSITY OF FLORIDA IN PARTIAL FULFILLMENT
OF THE REQUIREMENTS FOR THE DEGREE OF
MASTER OF SCIENCE

UNIVERSITY OF FLORIDA

2001

This thesis is dedicated to my family and friends, and in loving memory of James R. Wilkerson and James S. Blair.

ACKNOWLEDGMENTS

I would like to express my deepest gratitude to my advisor and committee chairman, Dr. Anthony Brennan, for his understanding, advice, and support during my time at the University of Florida. I would also like to thank the other members of my supervisory committee, Dr. Christopher Batich, and Dr. Ronald Baney, for their counsel and accommodation during this process. I am especially grateful to Dr. Laurie Gower, for agreeing to be a substitute member of my committee at such late notice.

The members of Dr. Brennan's research group have been a great source of advice, experience and camaraderie over the past two years. Specifically I would like to thank Jeanne Macdonald for taking responsibility of the lab and serving as group mentor and general well of knowledge. Licheng Zhao and Jeremy Mehlem both were valuable sources of experience and information. I would like to thank Adam Feinberg for his expertise with the AFM, SEM, and computer issues, as well as for his friendship. Chuck Seegert provided the wafers and the nuclear form method for this study, including a wealth of information on statistics, cell methods, and staining protocols.

Amy Gibson and Leslie Wilson provided the modulus data and the formulations for the modified elastomer samples. Their hard work and flexibility are greatly appreciated. Other members of the Brennan research group, Clay Bohn, Brian Hatcher, and Nikhil Kothurkar, have been an invaluable source of friendship and support. Paul Martin was always accommodating with regard to cell culture techniques and advice that was crucial to the completion of this work. I would also like to thank many other

graduate students in the Materials Science department and the Biomedical Engineering program, specifically Brad Willenberg, Brian Cuevas, Bob Hadba, Josh Stopek, Dan Urbaniak, and Jamie Rhodes.

I am indebted to Dr. C. Keith Ozaki and the members of his research group, specifically Zaher Abouhamze. Zaher was always helpful and went above and beyond the call of duty in assisting me at various times during this project. Dr. Edward Block graciously supplied the endothelial cells used in this study, and Bert Herrara was very generous and patient in supplying cells on a weekly basis. Nina Klingmann and Dr. Tina Lam were also a great source of information and I am grateful to Nina for allowing use of her incubators and cell culture equipment.

I would be remiss if I did not thank my family and friends who have supported me throughout this process and long before. My parents have provided me with every opportunity to succeed, and without their love and support, I could never achieve the goals that I have set. My wife, Laura, has been the greatest blessing and greatest friend throughout our relationship and especially during the first year of our marriage. Her understanding and support has no bounds, and her love has kept me going whenever I began to doubt. Most of all I would like to thank God for without Him, none of this would be possible.

TABLE OF CONTENTS

Page

LIST OF TABLES

LIST OF FIGURES

Figure Page

Abstract of Thesis Presented to the Graduate School
of the University of Florida in Partial Fulfillment of the
Requirements for the Degree of Master of Science

CONTRIBUTION OF MODULUS TO THE CONTACT GUIDANCE OF ENDOTHELIAL CELLS ON MICROTEXTURED SILOXANE ELASTOMERS

By

Wade Richard Wilkerson

December, 2001

Chairman: Dr. Anthony B. Brennan
Major Department: Biomedical Engineering Program

Contact guidance is a term used to describe a material's ability to direct the alignment and growth patterns of biological cells or tissue. It has long been understood that the surface a cell grows on impacts its size, shape, and metabolism. Typically, when cells are exposed to mechanical features such as ridges and grooves, the cells align and travel along the length. Surface chemistry plays a significant role in the attachment of cells to a substrate and in their movement on that surface.

The objective of this study was to study the effect of modulus as well as surface texture dimensions on vascular endothelial cells (ECs). To examine the effects of contact guidance on silicone elastomers, microtextured substrates were produced with reproducible and well-defined surfaces. Ridges of 10,000 μm length were fabricated at 3 different widths: 5 μm, 10 μm, and 20 μm, separated by 5 μm wide grooves to determine the effect of separation of features on the alignment of porcine vascular endothelial cells (PVECs). Two depths were examined: 5 μm and 1.5 μm.

Elastomer samples were examined with contact angles to determine their relative wettability and surface free energy. Formulations of elastomer with both functionalized and non-functionalized PDMS oligomer additives to alter the modulus were examined by contact angle, with no significant difference in surface energy. Surfaces were treated with fibronectin and radiofrequency glow discharge plasma in argon for 5 minutes at 50 W. Both treatments significantly increased the hydrophilicity after treatment, as measured by captive bubble contact angles. Dynamic contact angle analysis of textured surfaces showed a difference in smooth and textured areas as well.

Contact guidance of PVECs on textured silicone elastomers was measured by the nuclear form factor, in which the log of the ratio of nuclear length to width was presented. Results demonstrated that as the ridge width decreased from 20 μm to 5 μm contact guidance increased, as well as when the depth of the grooves increased from 1.5 μm to 5 μm. Data analysis showed that the groove depth was the most important factor in nuclear alignment. Contact guidance on fibronectin-coated elastomers was examined to determine the effect of modulus. It was expected that higher modulus materials would increase the effect of contact guidance. Elastic modulus on 4 elastomers was measured by tensile tests and resulted in a range of values from 0.3 MPa to 2.3 MPa. There was no significant difference in the contact guidance on the deep 5 μm grooves with varying modulus. The 1.5 μm deep grooves showed a significant increase in the alignment of cells to the groove in the highest modulus material compared to the lowest modulus material for the 5 μm and 10 μm wide ridges. The conclusion to be taken from these data is that modulus does seem to play a role in the determination of contact guidance, but other factors such as groove width and especially depth are more significant.

CHAPTER 1
INTRODUCTION

The ability to predict and control a biological response to a biomedical device would be a skill of dramatic technological and economic importance. Since man first attempted to replace nature's mechanisms and structures with artificial substitutes, he has met mainly with frustration marked with varying degrees of success. For implant materials, the factors that determine success are many, but the interaction between the surface and the surrounding tissue is one of the most important. The characteristics of that surface shape that interaction, and their secrets are slowly becoming known.

Contact guidance is a term used to describe a material's ability to direct the alignment and growth patterns of biological cells or tissue. It has long been understood that the surface a cell grows on impacts its size, shape, and metabolism. By determining the aspects of the material and the surface that influence contact guidance, there is a better opportunity to design a hierarchical system to elicit the desired response. Contact guidance can be controlled by topography and surface chemistry. Typically, when cells are exposed to mechanical features such as ridges and grooves, the cells align and travel along the length. The addition of roughness at certain levels can improve a biomaterial's ability to promote cell adhesion, while disrupting adhesion at different levels.[1-3]

Patterning surface chemistry on samples to change the wettability and surface energy has been very successful in controlling cell growth. Alternating strips or islands of adhesive proteins and materials with different surface energies have been examined. The incorporation of texture with surface chemistry allows for mutual interactions to

enhance the desired response.[2] As a better understanding of the principles involved is obtained, more subtle influences on the control of contact guidance can be examined.

The objective of this study was to study the effect of modulus as well as surface texture dimensions on vascular endothelial cells (ECs). ECs are important regulators of homeostasis in the human body, and a crucial component of the cardiovascular system. Diseases of this system currently contribute to more deaths than any other disease or cause. By controlling the alignment and growth patterns of these cells and their tissues, improvement of medical devices such as vascular grafts is possible. Modulus has been shown to play an important role in adhesion of biofilms on substrates in marine environments,[4, 5] and coupling the effects of modulus with topographical features is another important step in designing the behavior of materials.

The specific aims of this project involved the study of endothelial cells grown on microtextured silicone elastomers. Specifically, the effect of modulus was hypothesized to increase the effect of contact guidance as the modulus increased. This hypothesis was based on the observations of Kendall and others that modulus played an important role in the adhesion of biofilms on elastomer surfaces. These theories will be discussed in detail in the following chapters. To truly understand the system, another specific aim was to determine the importance of feature dimensions on this system. The hypothesis to be tested was that the depth of grooves in a surface played a more important role than the spacing between the grooves, and that a deeper groove increased the contact guidance of an EC on silicone. When the groove depth remained constant, the hypothesis being tested was that the grooves spaced closer together would improve the cells ability to direct cell growth. The importance of groove depth and spacing has been proven before

on different systems to confirm these hypotheses, but the effect of modulus on similar materials has not truly been examined.

To accomplish this objective, micropatterned silicone elastomers were fabricated with additives to change the elastic modulus while keeping the surface energy relatively constant. Surface topography was examined by various methods such as optical profilometry. Due to the low energy nature of the silicone, samples were treated with an argon plasma or coated with an adsorbed layer of fibronectin to improve cell adhesion. Porcine vascular endothelial cells (PVECs) were examined using the nuclear form factor, which is a measure of the alignment of a cell to defined topography by measuring the dimensions of its nucleus. The microtextured features were designed to be able to compare the degree of contact guidance by varying the feature width and depth. The modification of the samples with functionalized siloxane oligomers allowed for the variation of the modulus while studying the growth of cells on materials that are otherwise similar. These novel systems allow for the quantification of cell alignment, as well as a measure of a surface's capability for contact guidance

CHAPTER 2
BACKGROUND

Contact Guidance

The reaction of cells *in vitro* to the substrate they come into contact with has been traditionally separated into two main features: topography and surface chemistry. Cells adhere to surfaces via specific adhesion molecules that interact with proteins adsorbed onto the surface of the substrate. Thus, if the surface chemistry is favorable to adhesive protein adsorption, then the material should be favorable to cell adhesion. However, the topography of the surface is also important not only in the adhesion of the cells to the surface, but also in the behavior of the cells' metabolism and growth patterns after the initial contact. The purpose of understanding and controlling cell and tissue growth on artificial materials is to be able to design and implant medical devices that improve biocompatibility and functionality.

Surface Topography

The response of the cell to topography has been referred to as "contact guidance."[6, 7] The first known reference to the effect of substrate topography on growth characteristics comes from the growth of embryonic cells on plasma clots and spider webs.[8] Rovensky et al. used V-shaped grooves formed from copies of music records to show that chick embryo fibroblasts migrated from the bottom of the groove to the top over a period of hours and aligned along the texture.[9] Dunn and Heath examined chick heart fibroblasts growing on glass fibers to examine the effect of radius of curvature on

the cells.[10] They discovered an important aspect of contact guidance in that the shape of the substratum causes mechanical impediments to the formation of cytoskeletal bundles important for cell locomotion. By correlating this discovery with linear slopes and discontinuities, they determined that an angle of deflection greater than 8° between two planes of a prism affected their cells and made them less likely to cross over the ridge. Another important aspect of this paper introduces the use of the nucleus to quantify contact guidance, by factoring the elongation of the nucleus with respect to the orientation of a fiber. This technique will be used in the results portion of this thesis, and will be explained in more detail later.

Cells have also been shown to move along topographical features, and drastically change their morphology in response to this texture.[11-15] Clark et al. examined several cell lines in response to specific topography. They first examined baby hamster kidney (BHK) cells and embryonic neural cells in response to a single 5 μm step. Surprisingly, this is one of the only studies to examine such a simple topography. They found that the cells were inhibited from both climbing up as well as down the step, but tended to align along the ridge.[16] As a follow-up, they examined the same cells on grooved substrata of varying widths and depths (4-24 μm repeat width, 0.2-1.9 μm depth) and found that groove depth increased cell alignment and proved to be more important.[17] Similar results were found using rat bone marrow cells on poly-L-lactic acid (PLA) grooves, with an increase of extracellular material being deposited along the grooves.[18] Schmidt and von Recum show distinct morphology changes on pitted surfaces for macrophages and increased spreading on smooth surfaces.[19] Macrophages were also demonstrated to have the unique ability to align to extremely shallow grooves, from 30-70 nm.[20, 21]

The goal of substrate topography is to direct the cells to grow in a certain pattern and direction. Cells tend to align along a groove and move along this surface. Studies have shown that moderately porous materials improve cellular adhesion, which is possibly due to mechanical stability along with increased surface area for adhesion.[22-24] Endothelial cells (ECs) also have been shown to align along the direction of fluid flow.[25-27] In addition flow has been demonstrated to play a role in altering the mechanical properties of ECs. When subjected to a shear stress of 2 Pa over 24 hours, the endothelial cells gradually increased their stiffness as measured by the atomic force microscope.[26]

The methods of producing the precise surface morphologies vary depending on the size of the pattern and the material on which the pattern is being replicated. The smallest patterns are produced with direct write laser lithography[28] and AFM lithography while those on the 2-10 um scale are produced with UV photolithography, followed by reactive ion etching to control the slope of the walls.[2, 29-32] The most common method used in these experiments for producing features is to first lithographically produce the pattern on a silicon wafer, then replicate that pattern by embossing or spin casting onto the substrate.[33]

The grooves and ridges formed on these substrates have shown significant control over growth directions of cells. Current discussion focuses on the mechanisms behind the alignment of these cells to the surface topography. Von Recum and van Kooten question whether or not the actual geometries of the features are the defining factor, or the fact that there is a change in surface free energy due to edges and disruptions in the planar surface.[34] den Braber et al. concluded that parameters such as surface free energy and wettability influence fibroblast growth and proliferation on microtextured surfaces,

but not the shape or orientation of cells in comparison to the texture.[11] By SEM, they conclude qualitatively that there is more alignment on the 2 μm wide features, than on the 5 μm and 10 μm substrates. Other studies in this review seem to disagree with the their conclusion that fibroblasts do not align to wider features, but the fact that their groove depth was less than 1 μm seems to be a limiting factor. Walboomers et al. examined fibroblasts[35] and rat bone marrow (RBM) cells[18, 36] on polystyrene (PS) and PLA textured radio-frequency glow discharge (RFGD) plasma treated surfaces with ridges and grooves with dimensions varying from 1 μm to 10 μm wide and depths of 0.5-1.5 μm. These studies, along with another study they published demonstrated the importance of the ridge depth in that at deeper depths (up to 5.4 μm), the cells were more aligned, but not as many cells grew on the surface, even with the increase in surface area.[35] They also showed similar results in examining alignment of intracellular and extracellular proteins, but found that the addition of the ridges and grooves did not alter proliferation of cells on the surface at all.[12, 37-39] Their group also took their textured samples from *in vitro* use to *in vivo* by implanting RFGD treated disks of textured and untextured silicones subcutaneously in rabbits and guinea pigs, and PS disks in goats. Their results were mainly inconclusive, but they noticed with the silicone substrates an increase vascularization of the capsules surrounding the textured surfaces compared to the untextured surfaces.[40-42]

Typically, the more wettable the surface is, the more cell proliferation occurs. A study by Walboomers and Jansen et al. using rat dermal fibroblasts (RDF) on PS, PLA, silicone, and titanium coated PS substrates also show that the microtextures influence cell guidance, while surface chemistry influences morphology.[15] This study is of particular

interest, in that they examined the effect of different substrates with the same features. They compared the wettability of RFGD plasma treated samples and the elastic modulus to the substrate's ability to influence contact guidance. The features were the same dimensions as the previous studies, with the depth only 0.5 μm. The moduli varied from 894 MPa for PS to 0.39 MPa for silicone. Elastic modulus of 5 x 15 x 0.2 mm bars was measured using an Instron mechanical testing machine with a crosshead speed of 0.5 mm/s. A proliferation study showed no statistical difference in the number of cells attached to each surface, although there was a significant increase once each surface was RFGD treated. Contact angles using only water gave their measure of wettability, but their relatively high value for silicone (33°) after plasma treatment implies that the surface had rearranged or the plasma treatment was incomplete. This phenomenon will be discussed in more detail later. Their overall data were inconclusive, with their conclusions focusing more on the production of the patterns and the fact that different materials still induced contact guidance.

A more recent study by this group addresses the depth of groove issue, by examining epithelial tissue and cell migration across and along PS microgrooves.[43] Briefly, 6 mm punches of bovine eye endothelium were place on the microgrooved surfaces and cultured for 6-9 days. They studied ridges and grooves at widths of 1, 2, 5, and 10 μm and depths of 1 and 5 μm. This interesting study demonstrated the importance of groove depth, in that they concluded the width variations not to be as important as depth, but more importantly, they concluded that the microgrooves have the capability to direct tissue growth. By placing intact epithelial tissue on a patterned substrate, they found that on 5 μm deep ridges, the tissue was constrained to grow mainly

in the direction of the ridges and grooves, and did not cross over perpendicular to the features very significantly. Examples of explant growth and the distances measured are shown in Figure 2.1.

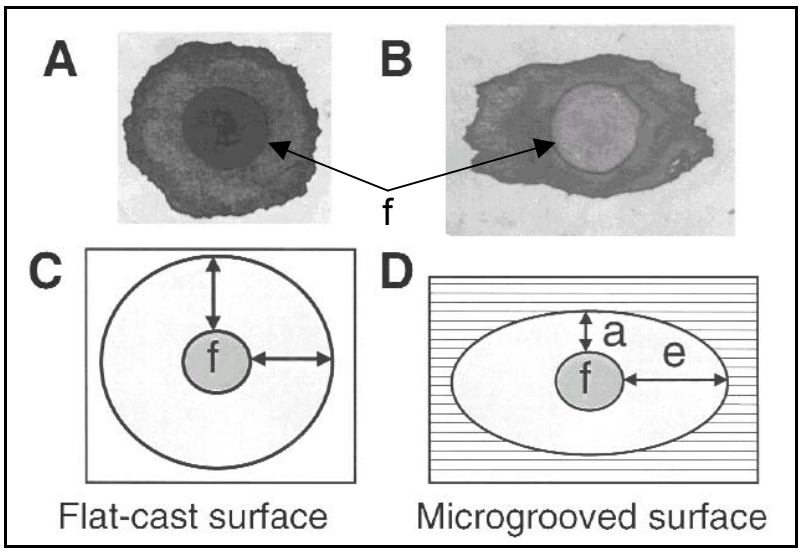

Figure 2.1 – Light micrographs and measurement protocols of 6 mm diameter punches of corneal epithelial tissue explants (f) over (A & C) smooth PS surface and (B & D) a surface with 1 μm deep microgrooves separated by 1 μm[43]

There was more growth perpendicular to the grooves with the 1 μm deep features compared to the 5 μm deep grooves, but the growth was still directed mainly along the feature direction. While the direction of the growth was more polarized with the 5 μm deep features, there was more tissue migration area for the shallower grooves. Similar results were found for cultured separated epithelial cells plated from a suspension.

The study of defined patterns of topography stemmed from many observations that the random roughness of a biomaterial surface influenced cell and tissue response. The phenomena of rugophilia and rugophobia, defined as cells loving or hating rough surfaces was initially pointed out by Rich and Harris.[44] The luminal surface of conventional Dacron vascular grafts can be considered textured in a random roughness

pattern. Studies in sheep have shown a distinct difference in the amount of cellular deposition on non-textured and textured polyurethane vascular surfaces after *in vitro* and *ex vivo* study.[45, 46] Using excimer laser micromachining, textured surfaces consisting of fibers of 25, 50, and 100 μm in length sticking up from a smooth base plane were examined. When implanted in ovine carotid arteries thrombus formed more quickly on the textured surfaces compared to the non-textured surfaces, leading the authors to conclude that the textured surface acted as a promoter of a stabilized thrombus base. While this may accelerate the formation of a stable pseudointima, the thickness and composition of the thrombus was not controlled.

Osteoblasts have also been shown to react more favorably to roughened titanium surfaces compared to smooth surfaces,[47] while surfaces with regularly spaced nanometrically sized pillars reduce tendon sheath (epitenon) cell adhesion.[21] This phenomenon is not seen for larger pillar sizes, in that astroglial cells showed preferential adhesion to pillars and wells on the scale of 0.5-2.0 μm in width and 1.0 μm in height.[48] In fact, 2 μm pillars and holes 4 μm deep showed changes not only in cell adhesion, but cell motility.[49] Neutrophils migrated much faster on holes than on smooth surfaces, while pillars slowed the process down.

A group out of Harvard headed by Vacanti has recently moved into using the effects of contact guidance and directed cell growth for future clinical applications. They used micromachining technology to form many branching networks resembling capillary beds. Hepatocytes and endothelial cells were patterned and lifted as 2D sheets for the purpose of forming 3D tissue constructs.[50] While this technique is far from perfected, it

is an interesting leap from the studying of contact phenomenon towards a more clinical application.

The field of contact guidance using topographical cues is quickly becoming more noticeable in clinical fields. Several excellent reviews have been authored and are a good starting point for an overview on the topic.[1-3, 51] However, topographical features are not the only tools for directing cell growth, as the chemistry of the substrates is becoming more popular in terms of directed cell growth and adhesion. As more studies are performed and a better understanding of the issues involved is achieved, clinicians and researchers are discovering the importance of the texture of medical implants as well as the chemical moieties on the surfaces.

Surface Chemistry

Surface chemistry plays a large role in the field of contact guidance for controlling the results of cell proliferation. Carter originally demonstrated that cells exhibit a preference to hydrophilic areas of patterned cellulose acetate and palladium metal surfaces.[52, 53] The cells migrated towards the metal and, in a separate study, along a gradient of metal concentration densities towards the more dense and thereby more hydrophilic areas. These studies were later duplicated and confirmed by Harris.[54] Currently, surface treatments are typically deposited in regular patterns using the same photolithographic techniques as with the topographical substrates. Self-assembled monolayers[55] (SAMs) and areas of enhanced adsorption of proteins due to surface energy seem to be the most popular. A study by Britland, et al. deposited a pattern of alternating hydrophobic dimethyltrichlorosilane groups with aminosilane groups on glass slides. No residual topography resulted and BHK cells showed a definite preference for the aminosilane sections, as the cells were crowded and aligned along the border rather

than cross to the hydrophobic groups.[56] A similar study was performed by Healy's group using human bone-derived cells (HBDC) and showed the same results.[57] Another study by Britland et al., examined the effect of topography in combination with surface patterning. This paper examined quite a few of the relevant topics with a few simple experiments, although their choice of cells (BHK) does not give as much useful information for the future. They superimposed tracks of aminosilanes orthogonal to the ridges and grooves and showed that for shallow grooves (0.1 μm to 0.5 μm), the cells aligned almost exclusively with the chemical patterning, but as the grooves go deeper up to 6 μm and closer together (5 μm), alignment to both the texture and the chemistry was seen.[58] By comparing these results with the studies on topographical patterning and chemical patterning, it is apparent that there are critical levels for each system, in which topography and chemistry contribute differently to contact guidance.

The use of silicones in the micropatterning of surfaces has also become quite popular.[59-63] Essentially, textured polydimethylsiloxane (PDMS) substrates are formed using the microfabrication techniques mentioned before. These substrates are then used as stamps or stencils to either directly apply surface treatments such as proteins to another substrate in an organized fashion, or to act as a mask allowing for microfluidics within channels in the silicone to pattern the surface.[59] Many times the silicone itself is the substrate that is used for cell studies. Whitesides' group has demonstrated that by selectively adsorbing adhesive molecules in the form of fibronectin to the bottom of pits or wells in the surface, and by keeping a non-adhesive protein like albumin on the surface above the wells, endothelial cells will adhere only to the bottom of the wells where the fibronectin is adsorbed.[64] They have also shown that through the use of microcontact

printing with PDMS stamps, they can pattern SAMs of alkanethiolates on gold to manufacture substrates with controlled islands of extracellular matrix (ECM). By restricting the size of ECM endothelial cells had to attach to, they controlled the size of the cell, which also resulted in altered metabolism.[65, 66] As the size of the area of attachment decreased, the cells changed from growth to apoptosis, or cell death. This technique is useful in its ability to isolate single cells on the same substrate for microarray examination of cell types.

Whether the application of a material is for a vascular graft, dialysis machine, blood oxygenator, bioreactor vessel, dental material, or the surface of a ship's hull, the first step in any biological response to a surface is the adsorption of proteins.[67-69] One cause of this adsorption is due to the highly varied structure of a protein in solution, both due to its conformation and primary structure of amino acids. Another cause is due to surface rearrangement of hydrophobic and hydrophilic areas of the polymer chain. In this fashion the surface properties and specifically surface energy play a very important role in protein adsorption.[70]

An adsorbed layer of serum proteins after exposure to blood is not in the same concentration as the bulk liquid. Rather each protein has a different response to the material in contact, as illustrated by Table 2.1. The composition of the adsorbed protein layer changes over time, as early adsorbing proteins are displaced by others, exhibiting the "Vroman effect."[71-73] Cells that adhere to a surface are able to deposit their own proteins, but only if the proteins are able to displace those already adhered. Hydrophobic materials, in the presence of high serum concentrations make this displacement very difficult.[34]

Table 2.1 – Enrichment of proteins adsorbed on polyethylene exposed to blood plasma[68]

Protein	**Enrichment**[a]
Fibrinogen	1.3
γ-globulin	0.53
Albumin	0.88
Hemoglobin	79
[a]Enrichment was calculated as the ratio of the surface fraction of the protein compared to the bulk fraction.	

Endothelial Cells

Endothelial cells make up one of the most important tissues of the body, known as endothelium, which is the interior lining of all blood vessels. The three major types of blood vessels are arteries, veins, and capillaries. Arteries and veins have a complex structure, made up of three main layers as seen in Figure 2.2. The outermost layer is known as the tunica adventitia, and is composed of loosely woven collagen fibers that protect and anchor the blood vessel. The middle layer, or tunica media, is mostly smooth muscle cells and elastin. This portion of the vessel is elastic and plays a major role in regulating blood flow by relaxing and constricting. The innermost layer is known as the tunica intima, and contains the endothelium on a subendothelial layer of loose connective tissue to act as a basement membrane.[74]

Cardiovascular endothelial cells (ECs) are diverse in their size and shape, since they are needed not only to act as a blood barrier in the aorta but also for nutrient exchange through tiny capillaries. For many years, endothelium was classified as an inert tissue, strictly a barrier to keep blood in its vessels. It is now known that the endothelium is an active tissue in homeostasis, producing factors such as endothelin, PDGF (prostaglandin-derived growth factor) and nitric oxide.[74] Endothelial cells are simple

squamous epithelial cells that form a smooth, confluent monolayer characterized by a cobblestone pattern, as seen in Figure 2.3.

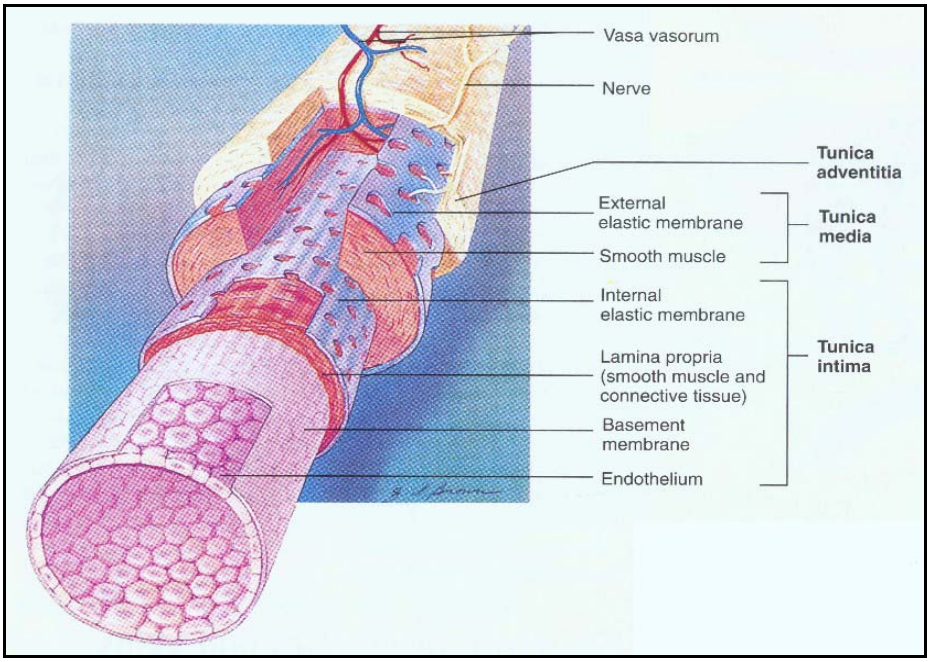

Figure 2.2 – Cutaway view of an artery showing the three main layers. From Seeley et al.[75]

As they achieve confluence, the cells are contact inhibited and alter their metabolic behavior, going into a period of stable growth and turnover, known as quiescence. In the adult, the average endothelial cell only divides approximately twice in a lifetime.[76] However, the endothelial cell can rapidly proliferate upon damage.

Disorders of the endothelium result in many pathologies, including atherosclerosis and cancer. It is generally accepted that a vascular graft or other blood contacting implant material will have less of an immune response if it is covered by an intact layer of endothelial cells. Endothelial cells effectively provide local delivery of endogenous endothelial secretory products to maintain prosthetic integrity after surgical

implantation.[77] When exposed to a topography that disrupts their ability to achieve confluence, the cells typically respond by moving on the surface and extending philipods out in multiple directions, searching for other cells and more favorable conditions.

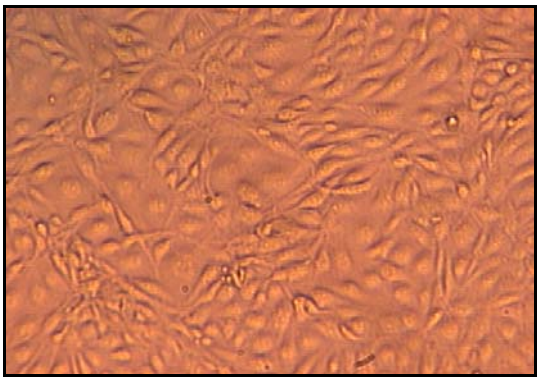

Figure 2.3 – Light microscopy image of confluent porcine vascular endothelial cells (PVECs) grown on tissue culture polystyrene (Image taken by L. Zhao and W. Wilkerson)

Vascular Grafts

In 1999, 529,544 people died from ischemic heart disease[78] and many undergo a procedure known as coronary artery bypass. This is necessitated by a blockage of the coronary arteries caused by fatty plaque accumulation or thickening of the artery wall. Coronary artery bypass graft (CABG) surgery is a procedure that supplies blood flow to the other side of the blockage by attaching a small diameter graft to the blood vessel. These grafts can take the form of native materials such as arteries and veins, or artificial polymers. The success and failure of these materials is crucial to the survival of the patient, and as of now no adequate small diameter vascular graft is available.

The typical treatment in a CABG procedure is to use the saphenous vein from the leg and the internal mammary artery as the graft materials. These are superior to non-

natural materials because they do not have an immune response in the patient and are more similar to the native tissue. These grafts have patency rates of over 70% after 5 years, while the survival rate without the surgery is nearly zero.[79] In cases where the autograph material is not available or unusable, then the only option is to implant a polymeric vascular graft. Large diameter vascular grafts used in aortic repairs are made from a woven polyethylene terephthalate (PET) mesh or expanded polytetrafluoroethylene (e-PTFE) and are very successful. PET is a thrombogenic material, in that it causes a cascade response that clots the blood at the surface of the graft. This response is actually favorable and encouraged, in that it seals the porous graft and since the aorta is such a large diameter blood vessel, the flow is not significantly diminished. To better control this process, the grafts are typically coated with albumin or collagen, essentially pre-clotting the graft.[80]

Small diameter artificial vascular grafts (< 6 mm) cause more of a problem in that the patency rate is less than 50% after 3 years.[79] Typically, the graft fails either due to thrombosis initially, or a buildup in the intimal layer of the blood vessel, essentially occluding the vessel with tissue. The thrombosis is due to the activation of the clotting cascade when the graft is exposed to the blood, activating platelets and the absorption of fibrinogen. Later in the life of the graft, the main threat to its success is occlusion by anastomotic intimal hyperplasia. The actual mechanisms of this are debated and are being examined, but a number of factors seem to contribute. First, there is a compliance mismatch between the native tissue and the graft. The artery has a very specific compliance to pressure waves during pulsatile flow that the graft interrupts. A mismatch causes stresses at the suture points of the anastomosis, which is typically where the

intimal hyperplasia occurs. This is the main cause of failure in autologous saphenous vein (ASV) grafts, due to the fact that arteries have a much more muscular vascular wall compared to a vein.[81]

Probably the most significant cause for the hyperplasia as well as thrombosis is the lack of a stable lining of endothelium, as in a normal vasculature. It typically only grows a short distance from the anastamoses, leaving exposed areas of pseudointima, consisting of fibrous materials and cells, including fibroblasts and smooth muscle cells. While current PET and e-PTFE grafts are inadequate in this regard, new materials are being investigated to improve cellular response to the tissues.[82-86]

An ideal graft material would exhibit thromboresistant qualities, have similar mechanical properties as the native tissue, have ease of use by the surgical team, and be able to form a stable endothelial layer. Currently the materials used are thrombogenic, have varying yet acceptable mechanical properties, are easy to use by surgeons, but do not form a stable endothelial layer.

Studies are in progress that have seen patency rates over two year periods double for artificial small diameter grafts due to endothelial seeding.[84] Currently, methods to improve endothelial cell seeding involve the adsorption of proteins on the surface or the use of fibrin glue.[22] Past results have shown that the substrate must tightly adhere the cells or they can be removed when subjected to shear flow. For surfaces without covalent linkages between the proteins and the surface or strong mechanical interlocking, it is difficult to form a stable intima that can withstand biological stresses. Many of these modified surfaces are attractive to proliferation of a fibrous pseudointima of fibroblasts and smooth muscle cells. With the proper surface chemistry and topography, endothelial

cell attachment and spreading to an intact, confluent layer that can withstand biological stresses should be possible.

Cell Adhesion

Focal adhesions are typically the main area of adhesion of a cell to a substrate. They are the link between ECM proteins such as fibronectin, vitronectin, and collagen adsorbed to the surface, and the cell receptors, known as integrins, which bind to the ECM through the well-documented Arg-Gly-Asp (RGD) tripeptide sequence. These receptors link the focal adhesions with the cell's cytoskeleton, thereby altering the cell's shape and locomotion. Focal adhesions are typically elongated, and oriented in the direction of the stress fibers and the main axis of elongation.[87] A recent study by van Kooten and von Recum have shown that fibroblasts and human umbilical vein endothelial cells (HUVECs) formed focal adhesions within the first 24 hr of adhesion on textured silicone surfaces.[14]

Recently work has been produced to examine binding polypeptide sequences to the surfaces of polymers.[88-93] The chemistry behind the grafting of these molecules on the surface can be accomplished by using plasma-induced graftcopolymerization. By exposing the surface to an argon plasma and then air, hydroperoxide groups are formed on the surface that can initiate radical polymerization.[92] Much work has been examined using the RGD sequence as the active adhesion area in proteins such as fibronectin. Hubbell examined the specific adhesion of endothelial cells to the Arg-Glu-Asp-Val (REDV) tetrapeptide through the $\alpha 4$-$\beta 1$ integrin and showed that while endothelial cells attach and spread on this ligand, fibroblasts, vascular smooth muscle cells, and platelets did not.[94, 95]

Recent work has refocused on the traction forces that cells impart on the substrate on which they adhere. By using low moduli micropatterned substrates,[87] and unpatterned "wrinkling" substrates,[96-100] studies have begun to quantify these forces for specific systems. Harris et al. first introduced the study of cell locomotion and adhesion with wrinkling substrates by growing a wide variety of cells on a thin, heat-crosslinked film of silicone floating on a silicone fluid. As the cells grow, they pull the film underneath in circumferential folds that are smoothed out when the cells are trypsinized from the surface.[96] Pelham and Wang were able to grow fibroblasts on polyacrylamide substrates with very low moduli but varying 12-fold. They found that fibroblasts spread less and had increased motility and lamellipodial activity on more flexible substrates, while more rigid substrates promoted stable elongated focal adhesions.[98] Surprisingly, this is one of the few studies examining the effect of different moduli of similar materials on cell growth, and none to date have been reported that compare the effect of modulus to the contact guidance phenomenon.

Balaban et al. used fibroblasts stained to expose the focal adhesions of fibroblasts grown on low modulus (E'~15 kPa) silicone elastomers with either fluorescent patterns embedded into the surface, or features similar to pits and pillars as part of the surface. The textures on their surfaces were 0.3 μm deep, because they wanted to minimize the contact guidance phenomenon. With features deeper than that, polarization and directed growth occurred along the features. In relating the displacement of the features with the locations of the focal adhesions, they were able to extract force measurements exerted by the focal points.[87]

It has been well documented that cell behavior, in the form of growth, movement, and metabolism, is closely linked to the shape of the cell.[101, 102] The effects of adding forces and changing the tension on a cell have shown significant changes in the biochemistry of the cell.[103] Several cell types also align along lines of principle strain with external loading.[13, 104] Kato et al. showed that endothelial cells, when patterned on thin strips of adhesive regions that caused endothelial cells to become elongated, exhibited a decrease in mRNA expression for vascular adhesion molecule-1 (VCAM-1) and a higher mRNA expression for intracellular adhesion molecule-1 (ICAM-1).[102] Topography has been shown to alter cell shape, fibronectin mRNA level and stability, and the secretion of ECM by human fibroblasts.[101]

In many cases, the shape of the cell is widely spread out, especially when lamellipods extend in multiple directions. This makes quantification of cell response to texture or chemistry difficult by simply looking at the outline of a cell. One approach has been to examine the shape of the nucleus of a cell to elucidate the prevailing cytoskeleton arrangement within the cell.[10] Ingber's group as well as others have demonstrated that the nucleus' shape is indeed directly "hard-wired" such that changes in surface adhesion can affect the shape and orientation of the nucleus.[105] They examined bovine endothelial cells after attachment to a substrate, and pulled on them with pipets coated with adhesion molecules and found that as the cytoplasm stretches, the shape and orientation of the ECs change from round to elongated along the stress.

As medical technology and surgical procedures improves, the need for effective biomaterials becomes greater. The ability of a non-native material to mimic the properties and functions of the tissue it is replacing is crucial to the success of the

prosthesis or device. Similarly, a biomaterial used in an *in vivo* or *ex vivo* application should minimize unwanted biological interactions.

Silicones

Silicones are widely popular materials and have many commercial uses today. They are unique in many of the polymers used in biomedical devices in that they possess a silicone-oxygen backbone instead of a carbon backbone. Their chemical and physical properties allow for their use in a variety of applications. The simplest silicones are polydimethylsiloxanes, a linear organosilicon compound whose structure can be seen in Figure 2.4.

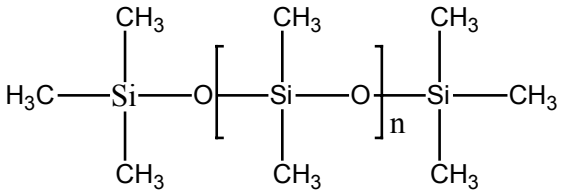

Figure 2.4 – Polydimethylsiloxane, trimethylsiloxy terminated

PDMS oils, when not cross-linked, are used in fields such as cosmetics, food-processing, and pharmaceutical preparations. Their lubricity and low surface tension make them excellent additives for anti-foaming.[106]

The methyl groups in the backbone and end caps of the PDMS molecule can be replaced by both functional and non-functional molecules, including hydrogen, phenyl, and vinyl groups. The significance of these substitutions is in their changes to the chemical and physical property of the polymer, as well as the curing and processing capabilities. Cross-linked PDMS forms a silicone elastomer that has excellent elongation properties (20-700%) and moderate breaking strengths (~ 1000 psi). They have been

cured in high-temperature vulcanizing (HTV) systems of methyl or vinyl groups using peroxides. Room temperature vulcanizing (RTV) systems are cured by condensing silanols with a moisture-sensitive silane cross-linking agent, or are condensed with a metal salt catalyst. Vinyl addition systems using platinum catalysts were initially used in low-temperature vulcanizing (LTV) systems, but has been extended to RTVs and HTVs.[106] The silicone used in this study is Dow-Corning's Silastic T-2, a filled RTV elastomer with vinyl terminated end caps that is addition polymerized with a platinum catalyst.

Use as a Biomaterial

Silicone elastomers are valuable polymers in the biomedical field. The use of silicone materials *in vivo* has become a heavily debated topic in the past decade, with the proliferation of procedures and studies on devices such as breast implants. These devices, made of a PDMS gel, allowed for the leaching or 'gel bleed' of low molecular weight oils from the device into the surrounding environment and then through the body. The silicone biomaterials were widely criticized for causing a large range of complications and diseases, and as a result, were removed from the market as a medical device. A recent risk assessment on the effects of silicone gel-filled breast implants concluded that the adverse effect of exposure to these prostheses was minimal, and current stringent regulation should be discontinued.[107]

One of the main problems with silicone implants, as with all implant materials, is the formation of fibrous capsules.[69] The capsules can cause discomfort as well as contraction on the device that can ultimately lead to failure.

Silicone's permeability to oxygen allows for their use in contact lenses and membrane oxygenators, and their flexibility and stability have seen uses in a wide variety

of implant materials.[92, 106, 108, 109] Silicone orthopaedic devices have included finger joints and temporomandibular joints (TMJ), which were not sucessful.[110] They have also been used in the vascular field as components to heart assist devices and incorporated into vascular grafts.[106, 111] While the mechanical properties of silicones are ideal for vascular grafts, in that their compliance and modulus more closely match the native tissue than PTFE or PET, their lack of toughness prevents them from being used exclusively. Also, a major concern with PDMS is its affinity for lipids, which causes it to become more brittle *in vivo* over time.[111] The important issue to keep in mind for silicone systems as well as other biomaterial applications, is that the bioactivity of the system will typically dictate what use the material has *in vivo*. Silicone surfaces are mainly non-thrombogenic and biologically inert, which makes them an interesting material to prevent unwanted interactions, but this lack of bioactivity also precludes it from becoming incorporated in surrounding tissues without surface or bulk modifications.

Another field of particular interest to our group is the use of silicones to prevent biofouling from marine organisms. Biofouling is an example of a problem concerning cellular materials accumulating on surfaces such as the hulls of ships and water treatment facilities. The marine spore *Enteromorpha* is the most common macroalga that fouls ships and submarines. Reproduction is mainly through motile spores that swim until a suitable surface on which to settle and adhere is located.[112] Adhesion involves secretion of a glycoprotein adhesive that anchors the spore to the surface.[113] Cues for settlement include phototaxis, chemotaxis and thigmotaxis. Previous anti-fouling coatings included biocides that did significant damage to marine life in harbors. Current research focuses on

preventing adhesion forces able to withstand the shear forces during motion.[114, 115] By using low surface energy silicones, coatings are foul releasing rather than antifouling. Singer and others in this field have realized the importance of the mechanical properties in determining the ability of a cell to adhere and remain adhered to a surface.[5] He simulated barnacle pull-off tests by epoxying a stud onto a silicone surface, and determined the critical force to pull it off with respect to the material's thickness and elastic modulus. The result was for lower modulus materials (E* = 3 MPa) and thicker coatings (up to 4 mm), the force needed to detach was less than for higher modulus (23 MPa) and thinner (0.08 mm) coatings. Gatenholm's group examined the use of microtextured surfaces in the marine biofouling environment by imparting 50-100 μm deep and wide features through use of a wire mesh as a mold. They found that barnacle adhesion on the macro scale decreased on textured surfaces compared to smooth. Many of these same principles of concern in biofouling can be used in biomedical applications to improve the biocompatibility of polymeric surfaces in the body.

Surface Energy

Due to its hydrophobic nature, silicone experiences rather high amounts of protein adsorption and poor spreading of cells.[92] Thus, to improve cell adhesion to a silicone surface, the chemistry of that surface is usually modified. Unmodified silicone is hydrophobic with advancing contact angles around 110-120°. The difference between the advancing and receding contact angle is known as hysteresis, and gives some understanding of a surface's ability to remodel itself as well as the surface roughness. As the silicone is exposed to water, hydrophilic areas of the siloxane backbone migrate to the surface, masking the hydrophobic methyl groups.[70] This provides a more hydrophilic surface and a lower contact angle while receding. This rearrangement of the silicone

backbone is an interesting phenomenon, and is especially important in PDMS systems due to its low T_g (-123°C). Most of the surface rearrangement in plasma treated high surface energy PDMS samples is due to the migration of low surface energy, low MW PDMS oligomers from the bulk to the surface.[116, 117]

Ostuni and Whitesides used the low surface energy of silicones to selectively pattern the surfaces of textured elastomer substrates with protein solutions. Since the contact angles of a fibronectin/physiological buffered saline (PBS) solution and a bovine serum albumin (BSA)/PBS solution on their silicones were over 100°, they could trap air inside of wells by carefully placing drops of the solutions on the surfaces. This allowed for the flat surfaces above the well to have one of the proteins adsorbed, and by rapidly changing the solution and adding a vacuum to pull out the air bubbles, the bottom of the wells were patterned with another.[64]

Schmidt and von Recum characterized Dow Corning's Medical Grade Silastic (MDX4-4210) silicone after texturing the surface with various pillars and wells. They determined the surface energy of their materials by using the stationary drop method[118] using diagnostic liquids that were not identified. They calculated Zisman plots that graph the cosine of the contact angle versus the surface tension of the diagnostic liquid. All of their samples, both textured and untextured had critical surface tensions of 20.5-21.5 dynes/cm.[119] They showed that the surface energy per unit of surface area decreased for higher densities of features, and concluded that the surface energy either was not greatly affected by their topography, or that contact angle methods are not sensitive enough to detect the difference.

Mechanical Properties

The importance of mechanical properties has been discussed in the uses for silicone materials and in the need for proper compliance for vascular graft applications. One area of interest is designing the mechanical properties to control the response of biofilms and tissues. Currently, the focus of our interest is in modifying the modulus of the elastomer without greatly affecting the surface chemistry or energy of the sample. Young's modulus, *E*, may be written as

$$E = \frac{\sigma}{\varepsilon}$$

where σ and ε represent the tensile stress and strain respectively.[120] Essentially, Young's modulus is a measure of the stiffness and compliance that is referenced in much of the biology-based research on these materials. The term compliance can be defined as the elongational compliance, *J*, which in regions far from thermal transitions is the inverse of Young's modulus.

$$J \cong \frac{1}{E}$$

This should not be confused with the compliance of vascular graft materials, which is a measure of the dynamic circumferential elastic properties of a vessel and is calculated using systolic and diastolic blood pressure and the vessel diameter by

$$C = \frac{\left(D_{systolic} - D_{diastolic}\right)}{\left(D_{diastoloic}\right) \times \left(P_{systolic} - P_{diastolic}\right)}$$

where D is the vessel diameter, P is the pressure, and C is the compliance.[121]

Typical glassy polymers such as polystyrene at room temperature have *E* values around 3 GPa, while soft rubbers are closer to 2 MPa.[120] PDMS based elastomers have a somewhat wide range of moduli, from 0.1 MPa to 10 MPa.[111] The change is due to the curing characteristics and the size of the oligomers, which affect the cross-link density, molecular weight between cross-links, and physical entanglements.

Currently, we are able to vary the modulus of our base Silastic T-2 elastomer over a range of moduli from ~0.1 MPa to ~3 MPa with the addition of functionalized and unfunctionalized PDMS oils. These oils can take the form of linear PDMS or larger "bulky" oils with side chains. By varying the molecular weight and functionalization of these additives, the variables mentioned above can be altered, without significantly changing the surface chemistry of the samples. The majority of the development and characterization of this system was performed by other members of the group, and so will not be discussed in great detail in this thesis. However, since the materials with differing moduli are of critical importance to the main purpose of this work, a description of the specific oils and testing methods will be discussed in the characterization section.

Research in our group has focused on the effect of mechanical properties on biofilm formation, whether the film is in the form of algal spores or endothelial cells. Kendall modeled adhesion behavior on elastomers by deriving formulae for the removal of rigid solids off of elastomers with varying thickness.[122] The critical pull-off force, P_c, required to remove a rigid cylinder with a radius of *a* from a film of thickness *t* is given by

$$P_c = \pi a^2 \left(\frac{2 w_a K}{t} \right)^{1/2}$$

where w_a is Dupre's work of adhesion and K is the bulk modulus, which is related to the elastic modulus, E, by Poisson's ratio, ν, by the following:

$$K = \frac{E}{3(1-2\upsilon)}$$

At greater thickness where $t >> a$, the relationship between the pull-off force and the elastic modulus is given by

$$P_C = \pi a^2 \left(\frac{8Ew_a}{\pi a(1-\upsilon^2)} \right)^{1/2}$$

The implication of this equation is that stiffer materials improve strength of adhesion.[5] One of the assumptions to this equation is that the attached surface is rigid, while for a cell, this is not the case. As discussed earlier with the low modulus wrinkling elastomers, a cell has the ability to create its own forces and change them depending on the substrate on which it is adhering. If a focal adhesion is modeled as a rigid body, then the equation can hold validity. If we imagine a cell applying traction forces on the substrate it is adhering to, then it is possible that a cell in equilibrium might exert forces just under the critical force in equal directions. Chicurel et al. concluded in their review of focal adhesion literature that a cell will continually contract on a substrate until the forces come into balance, much like a bow and a bowstring.[103] By that reasoning, for higher modulus materials the critical force is greater and thereby the traction forces applied. Since the ridges and grooves select the direction for a cell to align by directing its cytoskeleton, these increased forces would travel along the ridge and result in increasing the elongation of the cell, and the effect of contact guidance.

By examining textured surfaces with varying moduli while keeping surface energy variations to a minimum, this project attempts to minimize some of the unknown factors and study the effects of modulus on contact guidance. Before this can be completed, a thorough investigation of the surface topography and chemistry must be performed, and the results are discussed in the next chapter.

CHAPTER 3
CHARACTERIZATION OF SILICONE ELASTOMER SUBSTRATES

Introduction

The first step in this project was to fully characterize the silicone elastomers and textured substrates. Four separate formulations of silicone elastomer with functionalized additives and four with non-functional additives were used to vary the elastic modulus. The surface energy of each formulation was measured by contact angles of solvents with varying surface tensions. Dynamic contact angles in water were taken of the unmodified silicone elastomer with and without texture. Samples were treated with both radiofrequency glow discharge (RFGD) plasma and adsorbed fibronectin. Textured surfaces were provided at two depths of features, and the fidelity of the surface pattern was characterized by non-contact optical profilometry.

Materials

The base elastomer system, referred to in this thesis as "unmodified", is the *Silastic*® T-2 Silicone Moldmaking Rubber produced by Dow Corning. The resin is a dimethylvinyl-terminated polydimethylsiloxane (PDMS) composite mixture composed of PDMS and trimethylated silica for mechanical stability. It is a translucent resin that cures via addition polymerization with a platinum catalyst when added in a 100:10 ratio with the *Silastic*® T-2 curing agent. The typical properties of the base resin and elastomer system are given in Table 3.1. Resin was provided in 45 lb. containers and curing agent

provided in 4.5 lb. containers. To simplify the production, portions of the resin and curing agent were transferred into opaque HDPE bottles.

Table 3.1 – Typical properties of *Silastic*® T-2 Silicone Moldmaking Rubber (from Dow Corning product information sheet)

Test	**Unit**	**Result**
As Supplied		
Base Color		Translucent
Viscosity	Centipoise or mPa·s	50,000
Curing Agent Color		Transparent
Viscosity	Centipoise or mPa·s	550
As Mixed – 100 Parts Base to 10 Parts Curing Agent by Weight		
Viscosity	Centipoise or mPa·s	55,000
Specific Gravity		1.12
As Cured – 24 Hours at 25ºC		
Durometer Hardness, Shore A	Points	42
Tensile Strength	Psi	800
Elongation	Percent	300
Tear Strength, Die B	ppi	120
Linear Shrink	Percent	< 0.1

Two vinyl terminated linear PDMS oils and one bulky vinyl terminated oil were added to the resin to change the mechanical properties of the elastomer. A variety of non-functional PDMS oils of varying molecular weights were also examined for surface energy analysis. The molecular formula, viscosity, and molecular weight of each additive are given in Table 3.2. All were obtained from Gelest, Inc. and stored at room temperature. Five solvents were used for contact angle analysis: 1-Propanol (Aldrich, 99+% spectrophotometric grade), acetonitrile (Aldrich, 99.93+% HPLC grade), N,N-dimethylformamide (Aldrich, 99.9+% HPLC grade), diiodomethane (Aldrich, 99%), and

ultra-high purity DI water. Bovine plasma fibronectin was received from Sigma (cat # F-4759, 2 mg) as a lyophilized powder.

Table 3.2 – PDMS additives to silicone elastomer system

Name	**Molecular Structure**	**Viscosity (cSt)**	**MW (g/mol)**	**Catalog Number**
Vinyl terminated PDMS	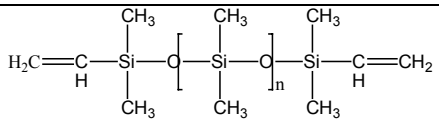	2-3 1000	550 28,000	DMS-V03 DMS-V31
Vinyltris(trimethyl-siloxy)silane	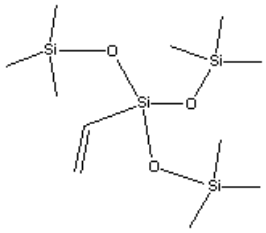	N/A	322.70	SIV-9300
Trimethylsiloxy terminated PDMS	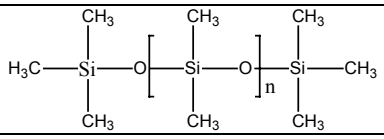	50 5000	3,780 49,350	DMS-T15 DMS-T35
Tris(trimethylsiloxy) silane	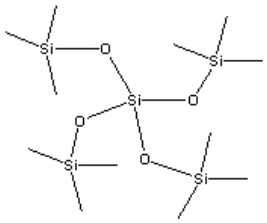	N/A	296.66	SIT8721.0

Methods

Elastomer Preparation

Unmodified elastomer substrates were produced according to manufacturer instructions. In a tri-cornered polypropylene beaker, resin and curing agent were added in a 100:10 resin to curing agent ratio by weight. The two components were mixed with a metal spatula until well incorporated. During the mixing process, many air bubbles were trapped in the resin, and so the mixture was degassed under vacuum for 10-15

minutes, periodically breaking the vacuum to rupture the bubbles formed. The uncured elastomer remains workable for approximately 1 hour.

For modified samples, oils were added to the resin before the addition of curing agent at the appropriate concentrations and mixed together. Curing agent was then added and the procedure was followed as above. For non-functionalized oils, the resin to curing agent ratio remained 10:1. For vinyl-terminated oils, the curing agent percentage was increased to account for the increase in vinyl groups. Unmodified samples were cured at room temperature, while vinyl-terminated samples were cured at 80°C for the appropriate amount of time, as seen in Table 3.3.

Table 3.3 – Curing conditions for silicone elastomer samples

Sample	**Curing Agent Needed**	**Cure Time and Temperature**
5% 2-3 cSt vinyl term (5% LMW)	0.16 x mass resin	4.5 hr at 80°C
5% 1000 cSt vinyl (5% HMW)	0.1011 x mass resin	2 hr at 80°C
15% vinyl tris	0.26 x mass resin	12 hr at 80°C
Unmodified and nonfunctional oils	0.10 x mass resin	24 hr at RT

Modulus Determination

Modulus values were obtained by Leslie Wilson and Amy Gibson and the values are used for material selection purposes only. A brief explanation of the method used is included here. Tensile specimens were made using an ASTM D1822-68 type L dogbone die, resulting in a 1-inch gauge length. Each sample was individually measured and the thickness of the samples was ~1 mm. Tensile measurements were made according to ASTM D412-97 on an Instron model 1122 equipped with the TestWorks 3.07 software for analysis. The dogbones were tested via crosshead displacement at a rate of 2

inch/min. Measurements of the modulus were calculated from the linear portion between the stress of 0.2 and 0.5 pounds and recorded.

Preparation of Textured Surfaces

All textured surfaces were taken from silica wafers with textures etched using microfabrication technology. Wafers were provided by Chuck Seegert at two etch depths, 5 μm and 1.5 μm. Briefly, silicon wafers were coated with a thin layer of a photosensitive polymer and then exposed to UV light through a photomask imparting various 5 μm patterns onto the photoresist as seen in Figure 3.1.

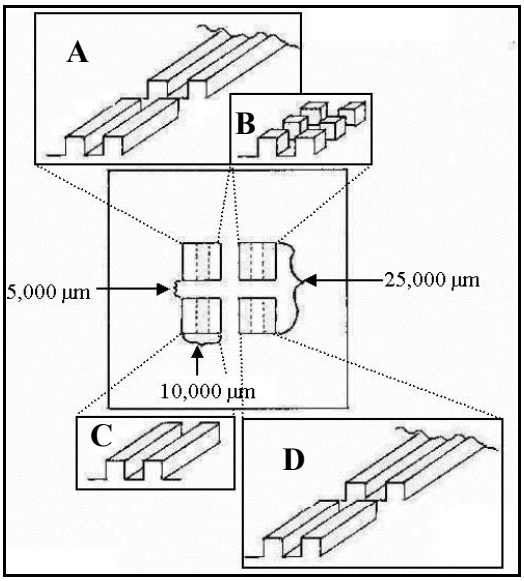

Figure 3.1 – Representation of etched patterns on silicon wafers. Each square side is 10,000 μm long and is made up of 5 μm wide ridges, separated by varying groove depth. Each square is separated into thirds with the groove depth in each third 5 μm, 10 μm, or 20 μm wide. Square A has ridges 60 μm long with 40 μm in between. Square B has 5 μm square pillars. Square C has 10,000 μm long continuous ridges and square D has 800 μm long ridges with 200 μm smooth space in between.

After development, the wafer was etched using reactive ion etching to the desired depth. The 5 μm deep wafer was patterned here at the University of Florida, and sent to Unaxis, USA for etching via the Bosch process. The 1.5 μm wafers were etched in

house. Each wafer was then glued to a metal backing with epoxy to improve mechanical stability. Before casting films for the first time, the wafers were treated with hexamethyldisilazane (HMDS) to minimize adhesion to the wafer.

Textured substrates were cast either directly on the wafers or on epoxy master copies. For the direct wafer copies, wafers were placed on a thin sheet of polyethyleneterephthalate (PET) taped to a glass plate and uncured elastomer was poured onto the wafer. Any trapped air bubbles were pierced with a needle. A second glass plate with a PET sheet and spacers was placed on top to form a constant thickness film of 3 mm. After curing, the plates were separated and the film removed from the wafer.

For the production of the epoxy master, PDMS copies of the wafers were made with an accelerated cure. The desired texture squares were then cut out and placed texture side down on a PET covered glass plate. Both 1.5 μm and 5 μm deep patterns were placed on the same plate. After positioning the textured surfaces, uncured elastomer was poured over the backside of the textured PDMS. The result was a PDMS film of constant thickness with individual squares of texture. This film was then used as a mold to cast epoxy (Epon 828 epoxy resin and Jeffamine D-230 hardener) over. The epoxy was cured at 80°C overnight and the PDMS film removed. The resulting epoxy master is a direct replica of the wafer texture. Unmodified textured surfaces were cast off of both epoxy and wafers, while modified silicones were cast mainly off of the wafers directly due to problems with adhesion to the epoxy at elevated cure temperatures.

Surface Treatment

Samples for the cell adhesion portion of this project were either left untreated, treated with a RFGD plasma, or coated with an adsorbed layer of fibronectin.

Radiofrequency glow discharge treatment

To improve the wettability of the substrate, surfaces were exposed to an argon RFGD plasma treatment. The plasma system used was a RF Plasma Inc. HFS 401S instrument, set at 50 W. Four samples in a polystyrene petri dish were treated at a time, approximately 5.5 cm from the bottom of the plasma RF coils, and after the samples were in place, the plasma chamber was evacuated for 10 minutes. Pressure in the plasma chamber got as low as 10 mTorr before treatment and typically around 25 mTorr immediately after the plasma was switched on. The argon gas was introduced at a flow rate of 200 sccm and the RFGD treatment was activated for 5 minutes. After treatment, the pressure was equalized in the chamber with ambient air.

Fibronectin adsorption

Fibronectin adsorption on microtextured elastomer samples was performed via the method of Ostuni and Whitesides.[64] Lyophilized bovine plasma fibronectin was received from Sigma and the contents were dissolved in 2 mL of 0.22 μm filtered water at 37°C for 45 minutes. The solution was diluted to 50 μg/mL in Hank's balanced salt solution (BSS). Elastomer samples cut into 15 mm disks were sterilized with 70% EtOH and rinsed 3X with BSS, then placed in 24-well culture plates and covered with 0.5 mL of the fibronectin solution. To ensure that fibronectin displaced air trapped in textured surfaces, the culture plate was exposed to house vacuum for 1 minute. During this time, small bubbles formed on the surface in the same pattern as the texture. After these bubbles detached, the vacuum was released and the fibronectin solution left on for 1 hour at ambient conditions. Samples were then rinsed three times with BSS.

Surface Energy

Untreated elastomers were examined for surface energy differences due to the additives. Sessile drop contact angles were measured for five solvents on each substrate. Five drops each of ultrapure water, methylene iodide (MeI), 1-propanol (1-prop), N,N-dimethylformamide (DMF), and acetonitrile (ACN) were measured for each substrate, and repeated on a second sample. Each drop was 2 μL as dispensed from a 25 μL pipet. An optical goniometer was used and the left and right contact angles were measured immediately after each drop was placed. Thus, 20 readings per liquid per sample were obtained. A Zisman plot was utilized to determine the surface energy of each substrate.

Captive bubble contact angles were taken on untreated, plasma treated, and fibronectin adsorbed unmodified elastomer. The substrates were placed treatment side down in a PMMA jar containing BSS. Bubbles of 2-4 μL of air were introduced into the BSS under the sample so they attached to the treated surface. Five bubbles for replicate samples were measured in the same manner as for the sessile drop method.

Dynamic Contact Angles

Dynamic contact angles were taken on a Cahn dynamic contact analyzer using the Wilhelmy plate technique. Briefly, Wilhelmy plate contact angles are taken by advancing and withdrawing a film into a liquid. The force on the film is measured and correlated to the film displacement. Textured and untextured unmodified elastomer and samples with non-functionalized PDMS oligomers were examined in ultra pure water in clean glass beakers. Samples examined were unmodified, 5% and 20% 50 cSt oil additive, and 5% and 20% 5000 cSt oil additive. Smooth films of measured thickness were cast in between glass plates with spacers. Textured surfaces were cast off polystyrene copies of the 5 μm wafer.

Films were cut into rectangles with dimensions approximately 10 mm wide and 30 mm long. The thickness was approximately 3 mm for the untextured films, but varied for the textured surfaces since they were cast off a PS copy with no back plate. Lower viscosity textured samples spread more and had decreased thickness when compared to the unmodified samples. The perimeter of the advancing cross-section was measured for each sample, and three samples were examined for each setting.

First, clean mica strips were dipped in the water at a stage speed of 100 μm/s. Surface tension of the water was calculated assuming perfect wetting of the mica. Textured surfaces were arranged so that 10 mm of untextured area is inserted into the water first, until 10 mm of textured lines running the width of the sample reached the water interface as demonstrated in Figure 3.2.

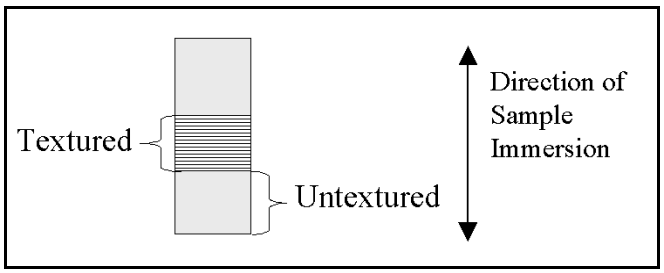

Figure 3.2 – Sample layout for textured substrates examined using DCA

Sample depth was set at 25 mm to include all texture and single dips were used for all samples. Advancing and receding contact angles were calculated for the smooth and textured areas using the Cahn DCA4A software package.

Optical Profilometry

Topographical characterization of both the textured elastomer samples and the wafers directly was performed using optical profilometry. The Wyko NT1000 from Veeko instrumentation uses non-contact interferometry with optical light to map the

surface in 3-D without affecting the surface properties or deforming the substrate. Magnification of the substrate can vary from 2.5X to 100X using the objective and field of view lenses provided. Samples were prepared as described above and needed no additional treatment. Both 1.5 μm and 5 μm deep samples and wafers were examined at 50X and 5X. The samples were leveled on the stage and focused before the scan was run. Profilometry data and 3-D rendering of the surface was accomplished using WYKO Vision32 version 2.210 software package.

Results and Discussion

Modulus Results

Since the silicone formulations and modulus testing was performed by others in the group, an extensive discussion on the theory and practice will not be included here. The samples were provided as materials that should have similar surface energies but with varying moduli. Figure 3.3 is a graph of the modulus of each material. Note that there are two values for the unmodified elastomer, one which is cured at room temperature, and one cured at 80ºC. It is important to note that the accelerated cure produced an almost 25% reduction in modulus. For this reason, all samples were cured at the set conditions for that formulation. The striped columns in Figure 3.3 represent the samples with functionalized additives. The 5% LMW and 5% HMW represents a 5% addition of the 2-3 cSt (~550 g/mol MW) and the 1000 cSt (~28,000 g/mol MW) vinyl terminated PDMS oils respectively. The 15% vinyl Tris is the lowest modulus material, and represents a 15% addition of the vinyl tris(trimethylsiloxy)silane molecule. The non-functionalized oils all decreased the modulus and should not have crosslinked into the network due to its methyl endcaps. The 20% 5000 cSt oil additive actually had a

"greasy" surface, where a film of oil that migrated to the surface was visible to the naked eye.

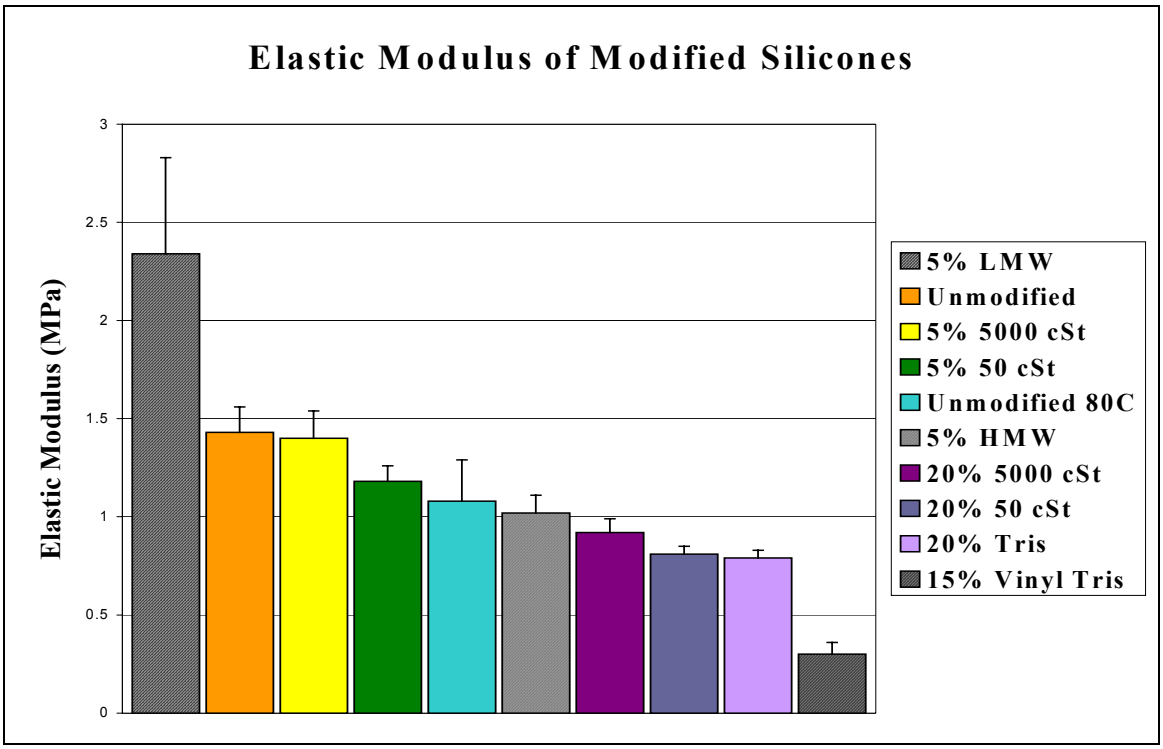

Figure 3.3 – Elastic modulus of modified silicones as measured by tensile testing. Striped bars represent elastomer with functionalized PDMS additives. (Data obtained by Leslie Wilson and Amy Gibson)

Surface Energy of Silicone Elastomers

As mentioned before, the surface energy of the elastomer formulations was determined using contact angles. Zisman and his group first introduced an empirical method of treating contact angle data to estimate γ_s, the surface free energy of the solid.[118, 123] The plot of $\cos\theta$ vs. γ_l, the surface tension of the liquid, form approximately a straight line with the formula

$$\cos\theta = 1 - b(\gamma_l - \gamma_c)$$

where γ_c is the critical surface tension, below which θ is zero and the surface is perfectly wetted. This is considered to be a measure of the surface free energy of the solid. The rationale behind this stems from Young's equation, represented as

$$\gamma_s = \gamma_{sl} + \gamma_l \cos\theta$$

where γ represents the surface tension (or free energy) and the subscripts s, sl, and l refer to the solid-vapor, solid-liquid, and liquid-vapor interfaces respectively.[123] Essentially this is a force balance between interfaces of a drop on a surface, with the solid-vapor and solid-liquid opposing each other in the plane of the solid. The basis of this theory is that with decreasing γ_l towards γ_s, then the solid-liquid surface tension is minimized and the solid-vapor surface tension will equal the liquid-vapor surface tension or surface free energy.

Contact angles were taken using the sessile drop method with 5 different liquids of known surface tension on the surface. Ten readings were taken for each sample and liquid by measuring the angle on both sides of the drop. The liquids used and their corresponding surface tensions can be found in Table 3.4.

Table 3.4 – Surface tension of liquids used for surface energy determination by contact angle analysis[124]

Liquid	**Surface Tension (mN/m)**
Water	73.05
Methylene Iodide (MeI)	50.76
N,N-Dimethylformamide (DMF)	37.1
Acetonitrile (ACN)	29.30
1-Propanol	23.78

Contact angles were measured for these liquids on unmodified elastomer, 5% LMW, 5% HMW, 15% vinyl tris, 20% tris, 5% 50 cSt, 20% 50 cSt, 5% 5000 cSt, and 20% 5000 cSt coated slides. For each sample, $cos\ \theta$ was plotted for each liquid versus the surface tension, and linear regression was performed to determine the surface free energy where $\cos\theta = 1$. The surface energy and contact angles of each substrate can be found in Table 3.5. A representative example of a Zisman plot from these data is shown in Figure 3.4.

Table 3.5 – Contact angles and surface free energy of various substrates

	Average Contact Angles (degrees)					γ_c
Samples	**Water**	**MeI**	**DMF**	**ACN**	**1-Prop**	(mN/m)
Unmodified	109 ± 4	67 ± 4	55 ± 2	47 ± 4	32 ± 2	19
5% 50 cSt	110 ± 3	66 ± 1	56 ± 2	44 ± 3	31 ± 1	20
20% 50 cSt	109 ± 1	64 ± 2	54 ± 2	46 ± 3	25 ± 1	21
5% 5000 cSt	108 ± 2	65 ± 2	55 ± 1	48 ± 2	26 ± 2	20
20% 5000 cSt	103 ± 2	64 ± 2	52 ± 2	48 ± 2	26 ± 2	19
20% Tris	106 ± 2	64 ± 2	56 ± 2	46 ± 2	29 ± 1	19
5% LMW	107 ± 5	65 ± 3	55 ± 2	47 ± 2	29 ± 3	19
5% HMW	112 ± 2	64 ± 2	56 ± 2	46 ± 3	25 ± 3	21
15% vinyl Tris	107 ± 2	66 ± 3	58 ± 3	50 ± 5	33 ± 3	17

As seen by Table 3.5, there is very little difference between all the samples in terms of surface free energy. This is an expected outcome since essentially the samples are all made of silicone elastomer with different PDMS oligomer additives. Since the material is the same, the surface energy should be similar. In addition, to minimize the energy at the interface, low surface tension oligomers have been shown to migrate to the surface.[116, 117] The fact that this does not affect a change in surface energy is supported by the results for the 20% 5000 cSt samples of no appreciable difference in surface energy even with a visible layer of oil on the surface.

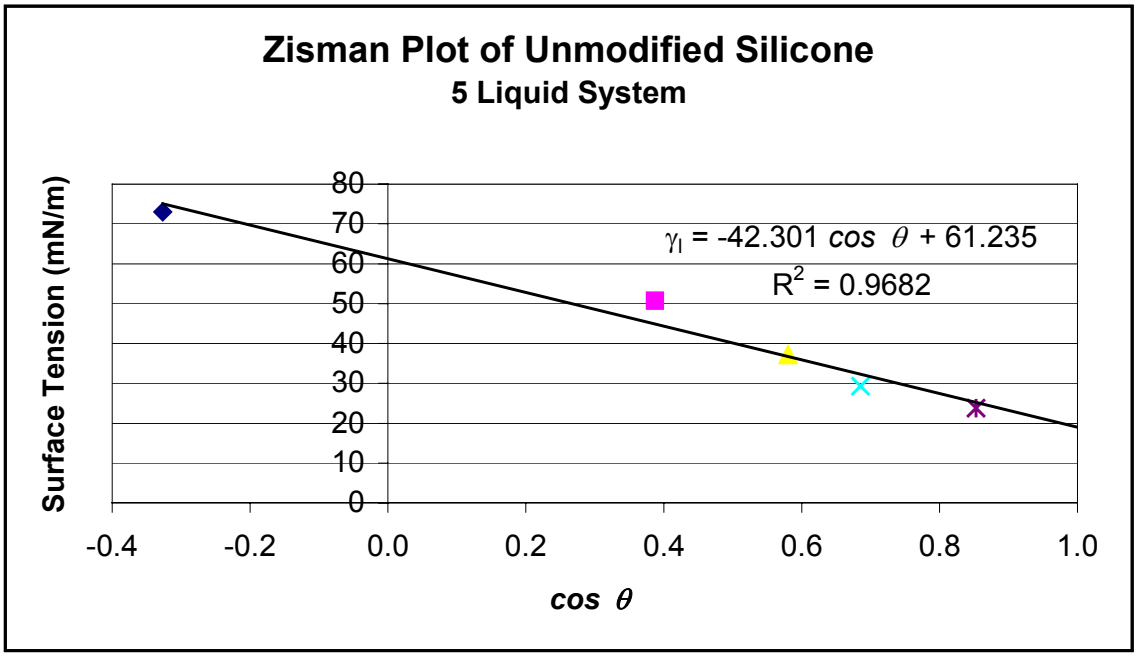

Figure 3.4 – Zisman plot of unmodified silicone for calculation of surface free energy

Contact Angles of Treated Surfaces

The two main surface treatments employed in this study are RFGD plasma treatment and adsorbed fibronectin. To determine the relative wettability of the surfaces, captive bubble contact angles were measured for plasma treated, fibronectin treated, and untreated unmodified samples. Results are reported in Table 3.6. As seen by the low angles on fibronectin and plasma treated surfaces, the hydrophilicity of the substrate has been greatly increased compared to the hydrophobic unmodified PDMS.

Table 3.6 – Captive bubble contact angles on treated surfaces

	Contact Angle (degrees)
Unmodified	87 ± 4
Fibronectin treatment	15 ± 4
Plasma treatment	< 10

Plasma Treatment Issues

The fibronectin-coated surfaces change their hydrophilicity by adsorbing a layer of protein on the surface, but the plasma treated samples modify the surface chemistry of the base polymer. The literature implies that two factors seem to be at play here. One is the modification of the surface by creating free radicals that when exposed to air form peroxides on the surface.[92] This is the method used to add adhesion molecules and other chemistry to the surface through graft copolymerization. However, as the plasma treatment increases, an oxidized silica-like layer forms on the surface, especially if the plasma contains oxygen. This is typically a problem when using silicone coatings as high-voltage outdoor insulators. Studies have shown this silica-like layer to be up to 150 nm thick on the surface. This layer eventually cracks and then allows the low MW oligomers to migrate to the surface.[116] This was not considered to be a problem with the plasma treatment of the samples, but in analysis of the surfaces it was noticed that many of the plasma treated elastomers had cracks. These were not seen after removing the samples from the plasma chamber. As the samples were peeled off the dish to be placed in the wells, cracks were formed that were not there before or immediately after treatment.

The main concerns with this phenomenon is the influence the cracks would have on the cells compared to the intended topography and the effect that a harder silica-like surface layer would have on the modulus. To examine this affect, a textured sample of 15% vinyl tris silicone was plasma treated under the same conditions as the samples and examined using optical profilometry and atomic force microscopy (AFM), as seen in Figure 3.5, Figure 3.6, and Figure 3.7. The sample was bent to simulate removal and

placement in a culture dish. Cracks on the order of 0.5-1.0 µm were observed, and appeared mainly as positive textures pushing up from the surface. Since the transformation of the material from PDMS to a silica-like oxidized layer results in a large decrease in specific volume, tensile stresses are formed in the oxidized layers. These stresses are relaxed by the cracking and result in an elevated texture, as seen and explained by Hillborg, Sandelin, and Gedde.[116]

Of concern also is the affect that the plasma treatment has on the shape and size of the features. Profilometry data presented in Figure 3.8 shows a very dramatic change in the height of the ridges, changing from 1.43 µm to 0.81 µm. It is apparent that the plasma treatment at this level is ablating the surface and seriously altering the features.

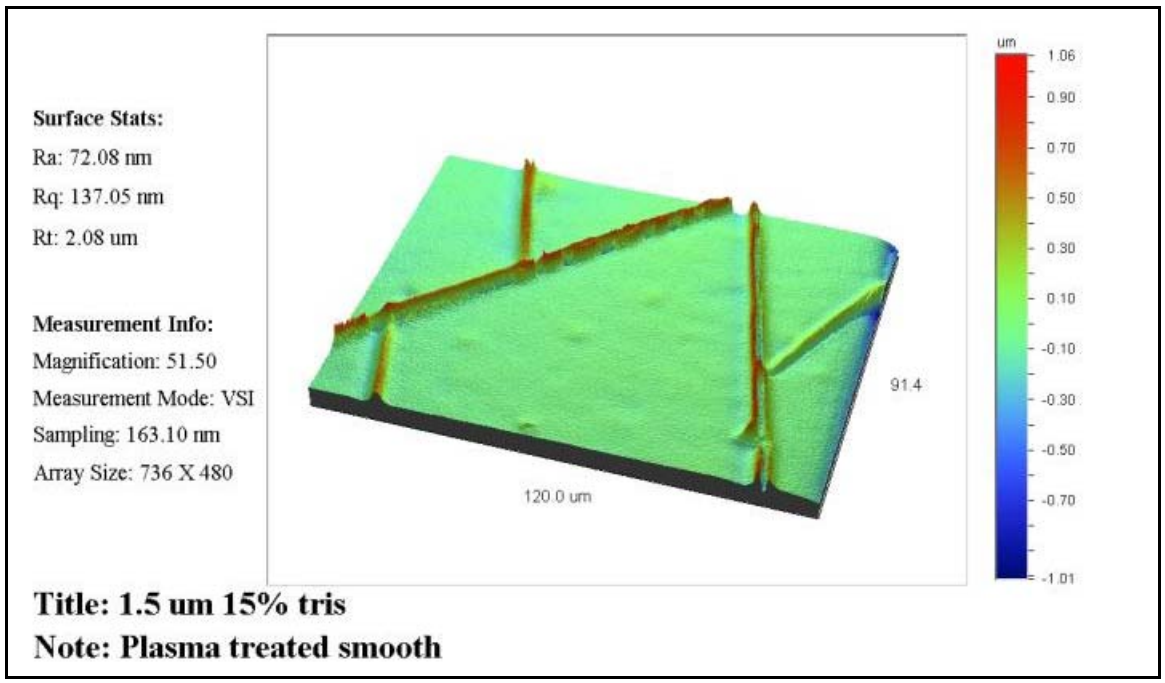

Figure 3.5 – Profilometer image of surface damage due to plasma of 15% vinyl tris textured elastomer sample (smooth area)

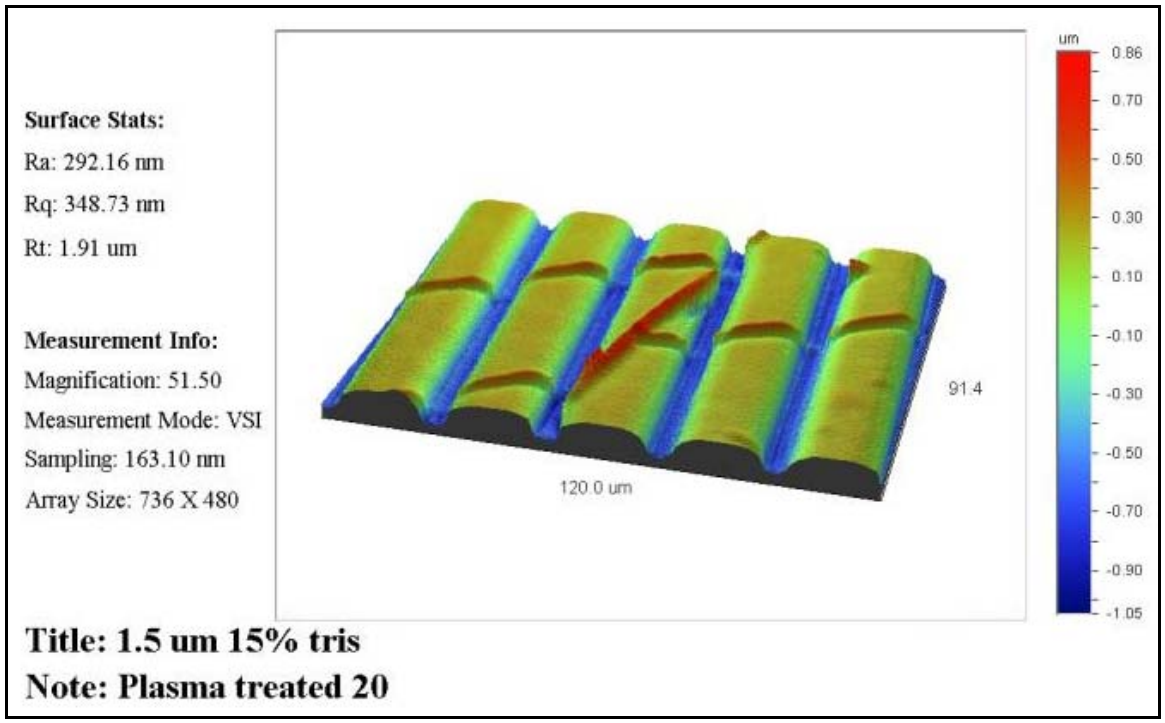

Figure 3.6 – Profilometer image of surface damage due to plasma of 15% vinyl tris textured elastomer sample

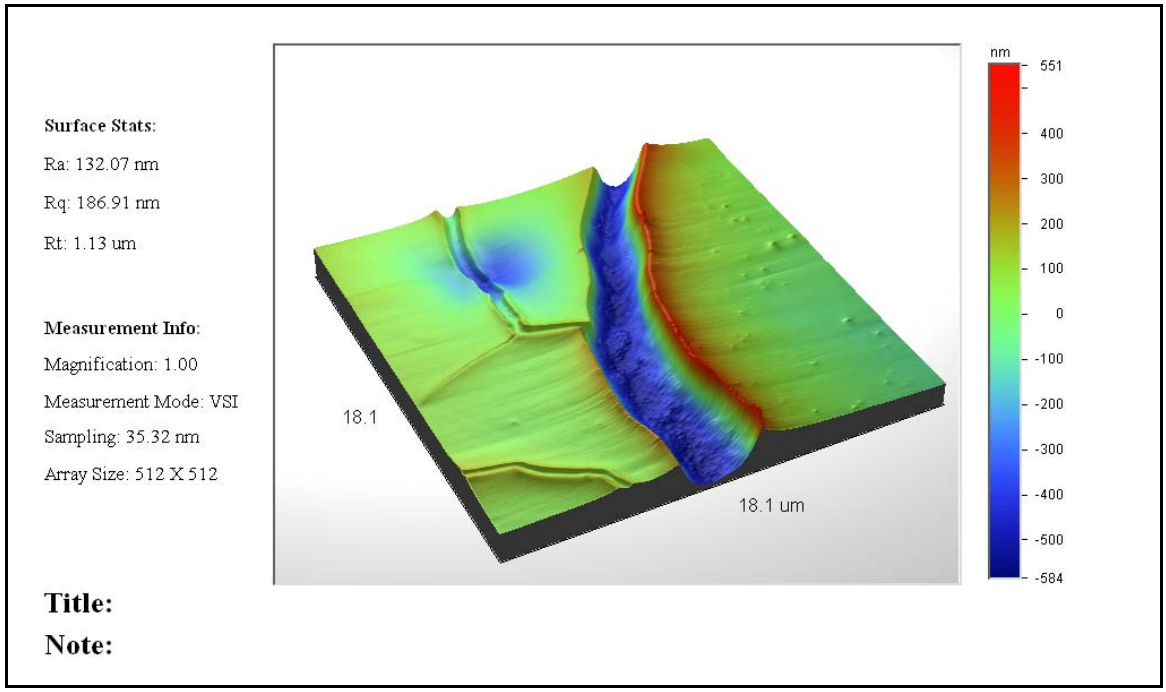

Figure 3.7 – AFM Image of crack on plasma treated sample

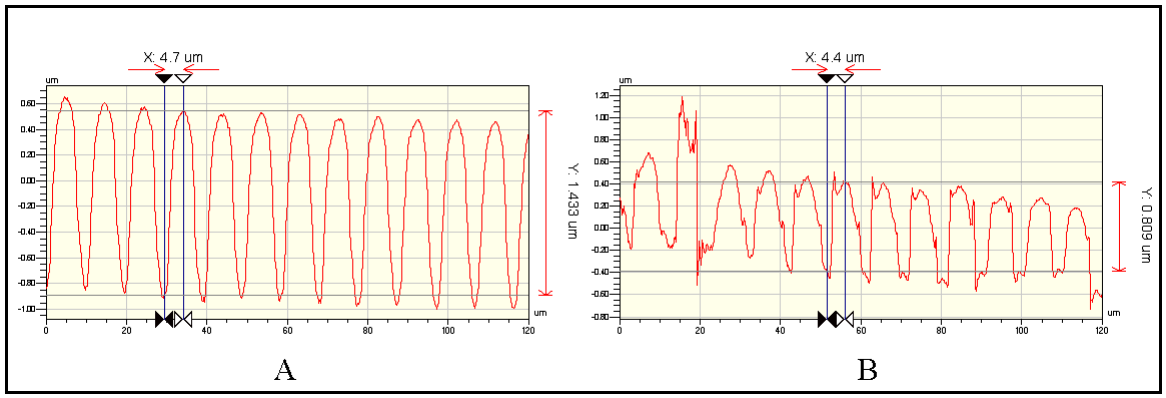

Figure 3.8 – Profilometry data for non-treated (A) and plasma treated (B) 1.5 µm deep elastomer textured surfaces at the 5 µm width spacing. Height of ridge: A = 1.433 µm, B = 0.809 µm.

Another feature of using a silicone surface is the effect of rearrangement of the surface properties due to mobility of the chains and migration of low MW oligomers. To examine this effect, unmodified elastomer samples were treated at two plasma power levels, 50W and 100W using the same procedure as in the methods section of this chapter. Contact angles of water on plasma treated samples were examined using the sessile drop method immediately after treatment, 15 minutes after treatment, and one week after treatment and the contact angles reported in Table 3.7.

Table 3.7 – Water contact angles on plasma treated silicone samples after exposure to air over time

	Average Contact Angles (degrees)	
Treatment conditions	**50 W, 5 min**	**100 W, 5 min**
Before Treatment	103 ± 8	114 ± 3
Immediately after treatment	< 10	<10
15 minutes after treatment	15 ± 4	<10
1 week after treatment	77 ± 7	45 ± 28

The data indicate that with the more intense plasma treatment, the hydrophilicity of the surface is more stable over a period of a week, however, the high standard deviation after 1 week exposure to air for 100 W sample implies that the surface has areas of homogeneity that are rather extreme. Some areas had contact angles as low as 25° while others had angles ~80°. The stability of the surface is possibly due to a silica-like crust as mentioned above, and the areas of hydrophobicity are due to low MW oligomers migrating through cracks.

Dynamic Contact Angle

Dynamic contact angles are taken by advancing or removing a liquid interface on a surface. This can be accomplished with a variation of the sessile drop method by either adding or subtracting fluid, or by tilting the plate and measuring the angle. Another technique is the Wilhelmy plate method, where a film of material is dipped in a liquid and the force on the plate is measured. The force is related to the surface tension of the liquid by the equation:

$$F = \gamma_{lv} P \cos\theta$$

where P is the perimeter of the plate. By measuring the force and perimeter of a sample in a known liquid, the contact angle can be determined for both advancing (inserting) and receding (withdrawing) contact angles.

Dynamic contact angle data was taken on unmodified silicone and the linear non-functionalized additives. Functionalized oligomers were not available at the time of examination and the method of production had yet to be determined. In addition, samples with both smooth and textured areas were examined. Figure 3.9 is a representative force-distance curve taken from DCA data. The lower linear portion of the curve represents the

advancing or inserting portion of the dip. The force values are negative due to the fact that the low-energy surface is resisting being wetted by the water, and in essence a reverse meniscus is pushing up against the sample. The upper linear portion is the receding area of the curve. The separation of the two curves is a measure of the hysteresis, or the difference between the advancing and receding contact angles, represented as $\Delta\theta$ in Table 3.8. The slope of the linear portions is due to a buoyancy effect and is factored out by extrapolating the line to the point of sample contact with the water, or zero depth of immersion (ZDOI).

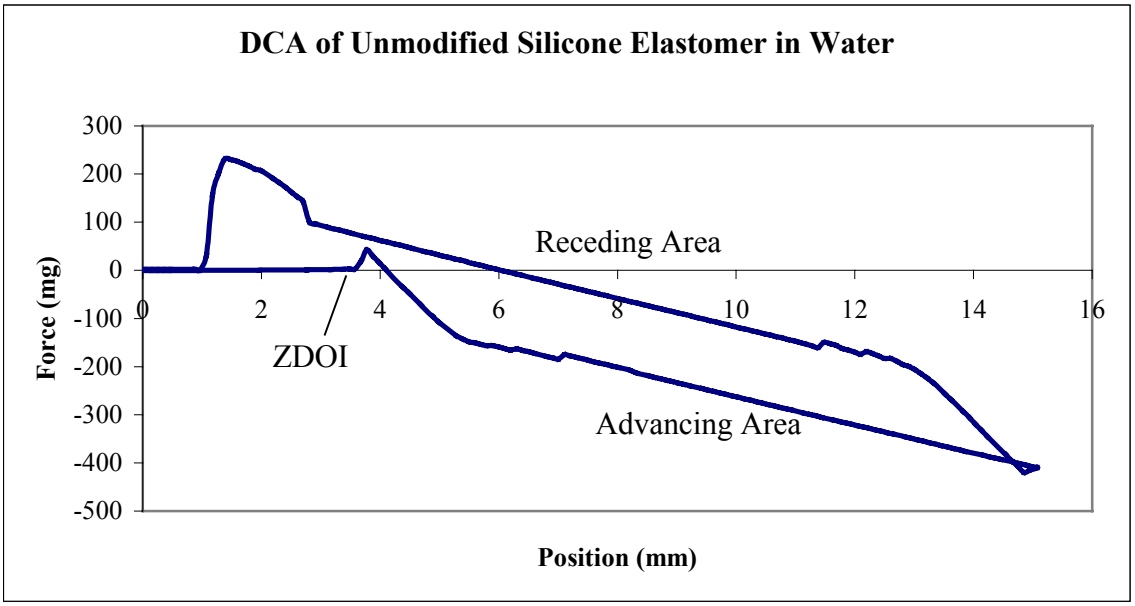

Figure 3.9 – Force-distance curve from DCA of unmodified silicone elastomer in water

Hysteresis is caused by multiple factors, especially roughness and surface heterogeneities. For most smooth surfaces, roughness under 0.5 μm contributes minimally to the hysteresis of a sample.[125] Hysteresis due to rearrangement of the polymer backbone so that more hydrophilic moieties are exposed to the surface play a large role in the decrease of receding contact angles compared to advancing.[123, 125]

Essentially, as the surface is in the receding phase, the meniscus is traveling over a previously wetted surface with a different surface energy than before. Due to this phenomenon, the advancing contact angle can be considered a measure of the low-energy portion of a heterogeneous surface and receding angles are more characteristic of high-energy parts.[125] In examining Table 3.8, one aspect that stands out is the small hysteresis of the 20% 5000 cSt samples. This is most likely attributed to the fact that these samples had a visible coating of oil on the surface, which may mask the rearrangement process, or at least minimize the effects.

Table 3.8 – DCA data on silicone elastomer modified with non-functionalized PDMS oligomers

Viscosity	**Wt. %**	θadv	θrec	$\Delta\theta$
Unmodified	0	115.1 ± 3.8	68.7 ± 2.2	46.4 ± 1.7
50 cSt	5%	113.9 ± 1.8	77.5 ± 1.8	36.4 ± 0.3
50 cSt	20%	100.5 ± 1.3	65.1 ± 2.1	35.4 ± 1.6
5000 cSt	5%	106.1 ± 0.7	71.6 ± 2.2	34.5 ± 2.1
5000 cSt	20%	101.0 ± 0.8	89.4 ± 4.4	11.6 ± 4.4

Figure 3.10 is an example of a force-distance curve taken on a textured substrate. The sample advances into a smooth area, and then into an area of texture. At the end of the advancing dip, the sample is retracted through the textured area and then on to the smooth area. Several factors preclude the presentation of numerical results for this study. For many samples, the lengths of smooth and textured areas were not long enough to achieve a linear region of stable contact angles. In addition, the varying thickness and the fact that only one side of samples were textured make numerical contact angles unreliable. However, for the majority of the samples, the trend was similar. The advancing textured areas had higher contact angles than the smooth areas, while the

receding textured contact angles had wide variations. Due to the high aspect ratios and significant roughness of the textured areas, air is trapped in the grooves when the advancing front of the liquid passes over. As can be seen by Figure 3.10, the advancing force decreases as the liquid front reaches the texture, which in effect is increasing the resistance of the water to the film penetration. As it encounters areas of low surface energy air trapped in between the grooves, the water adheres to the ridges until the surface tension is overcome and it can bridge to the next ridge.

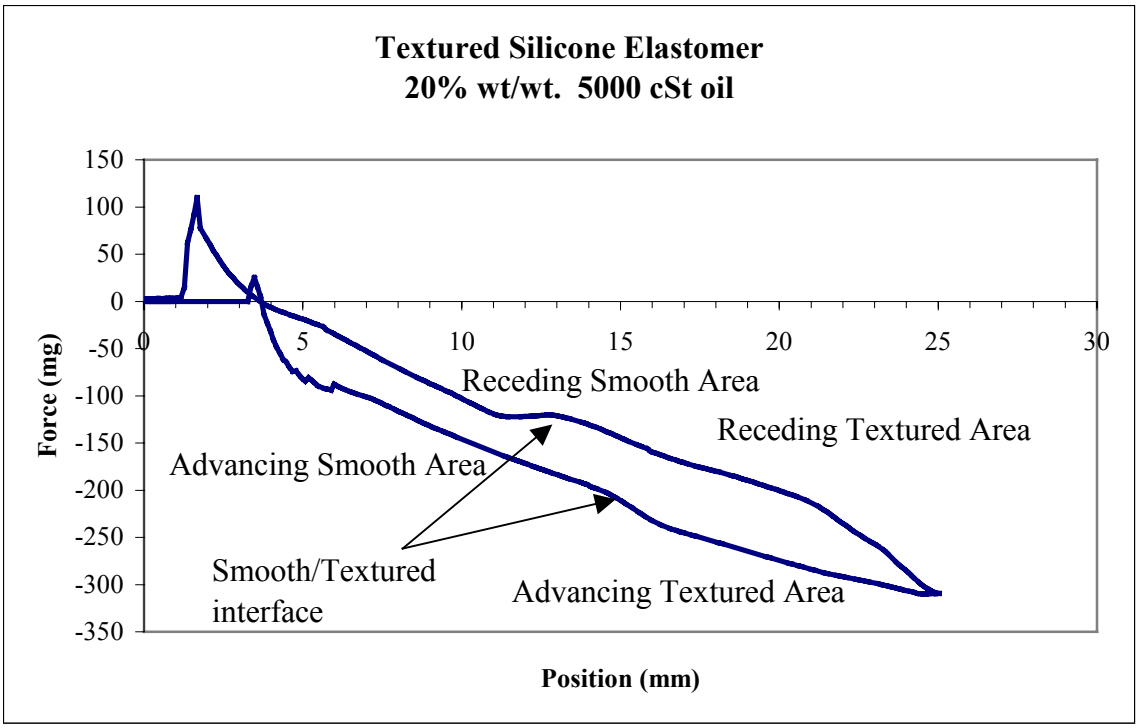

Figure 3.10 – Force distance curve from DCA on a textured silicone elastomer substrate

Optical Profilometry

Optical profilometry is a useful tool for characterizing the shape and 3-D features of textured substrates. It uses white light interferometry to determine the topography of a substrate without contacting the surface. It also has the great advantage that no surface

modification or contact is necessary to take measurements. Imaging procedures like SEM require a surface coating and high-energy treatment of the surface, which may change the properties as well as rendering the sample itself unusable in the future.

Figure 3.11 shows representative 3-D renderings of an unmodified silicone copy off the 5 µm deep textures. Figure 3.12 includes profilometry images taken directly off the wafer for comparison. The textures in Figure 3.11 were replicated from epoxy, demonstrating the ability of the epoxy system to faithfully recreate the wafer's features. Note that these copies are in effect the "negative" of the wafers, in that the ridges have varying widths and the grooves are a constant width and depth of 5 µm.

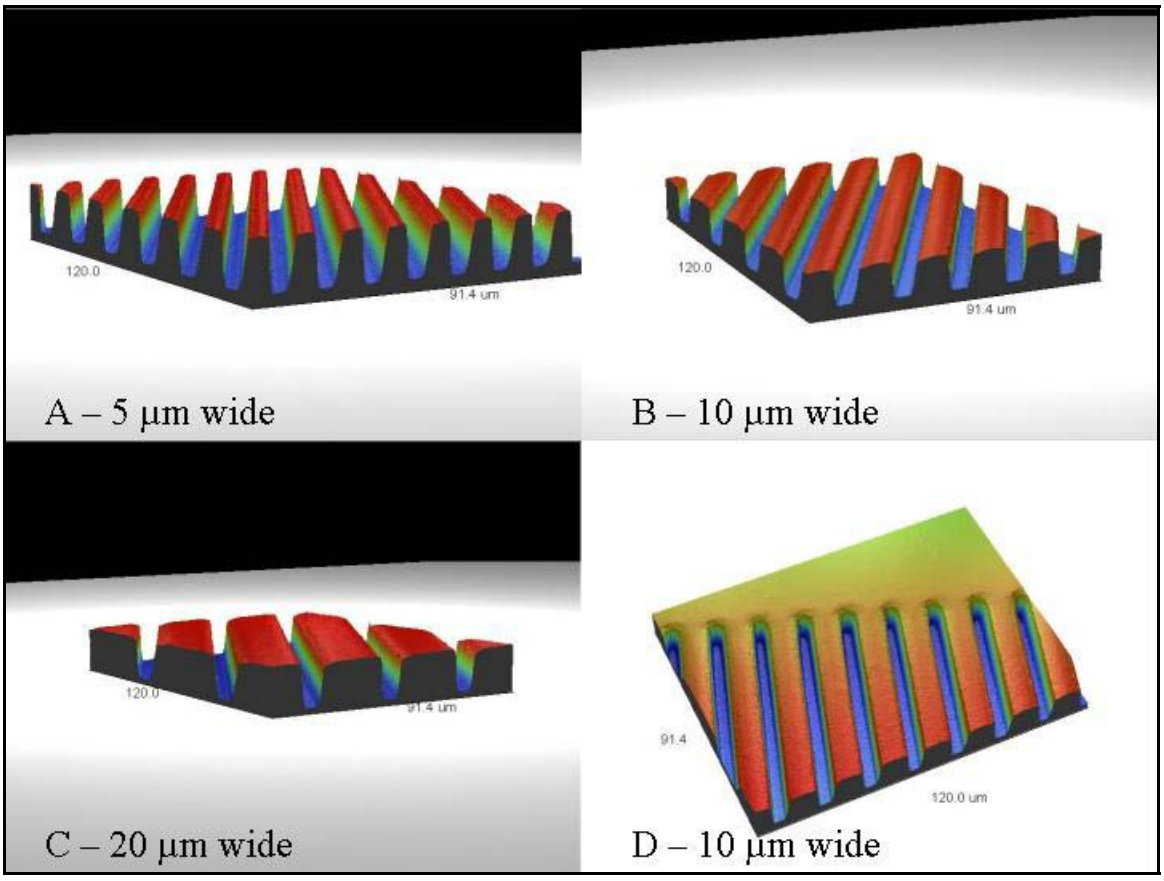

Figure 3.11 – 3-D images of 5 µm deep elastomer samples copied off of epoxy taken with optical profilometer (50X). (A-C) are examples of the ridges at the different spacing. (D) demonstrates the smooth/textured interface

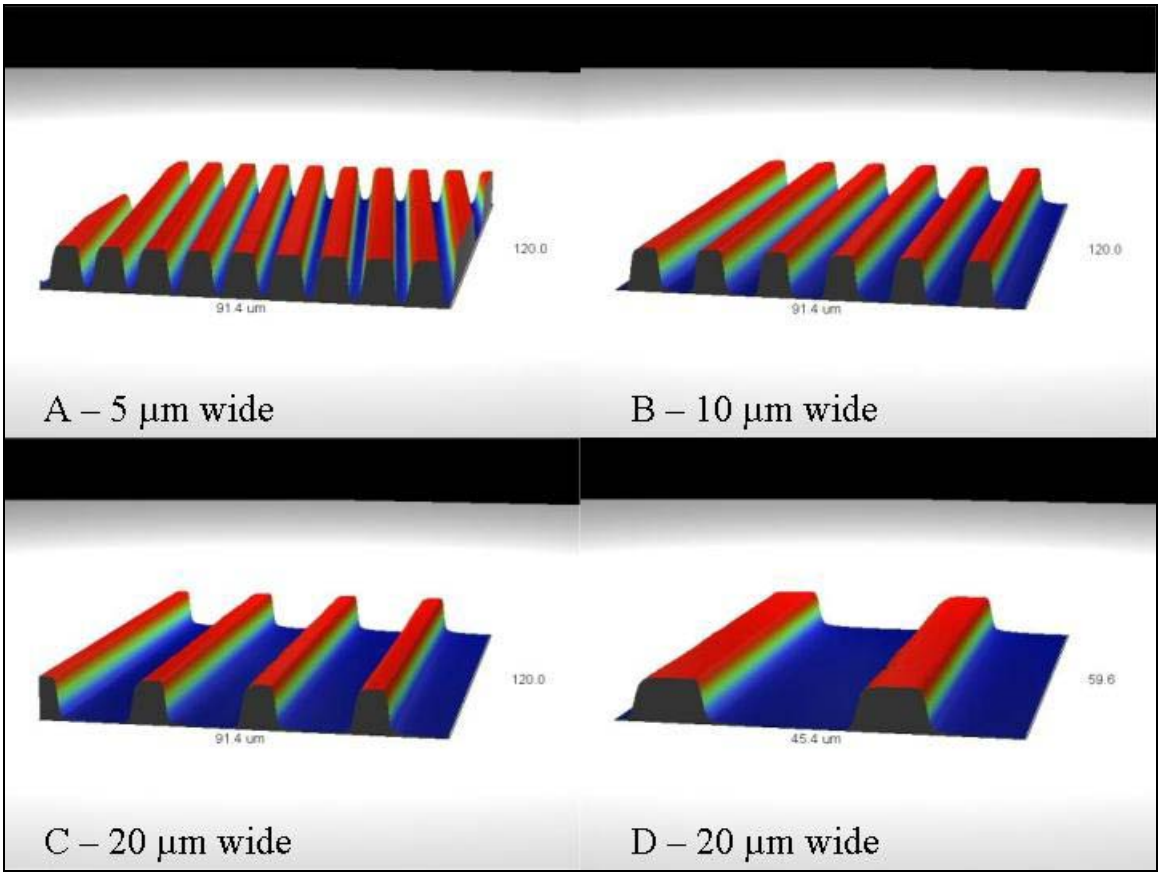

Figure 3.12 – 3-D images of 5 µm deep etched silicon wafers at each width spacing, taken with optical profilometer. (50X A-C, 100X D)

Figure 3.13 is an example of the features from a 1.5 µm deep wafer. These were cast off the wafer with 5% LMW elastomer and cured at 80°C. The left side of the image is elastomer copies of the wafer, which is represented on the right side. Replication is good, but the shape of the 1.5 µm ridges are more rounded and pointed at the top after replication (see Figure 3.8A for 2D profilometry of 5 µm spacing). Table 3.9 gives the quantitative values for ridge depth and width taken with the optical profilometer. All of the ridge widths for the wafers are 5 µm since the groove spacing is varied. This translates to variations in ridge spacing for the elastomer copies. What is apparent is that

the etching process does not give perfectly spaced features, especially with the 1.5 µm wafer. The 5 µm deep wafer has better retention of expected ridge values, most likely due to a more controlled reactive ion etching process.

Table 3.9 – Optical profilometer data of ridge widths and groove depths of the 1.5 and 5 µm deep wafers and elastomer copies. The wafers should have a constant ridge width and the elastomer copies have ridge widths of 5 µm, 10 µm, and 20 µm.

Sample	Ridge Width (µm)			Groove Depth (µm)
5 µm wafer	4.8 ± 0.1	4.9 ± 0.2	4.9 ± 0.2	5.3 ± 0.2
5 µm elastomer	4.7 ± 0.1	9.2 ± 0.4	19.1 ±0.1	4.9 ± 0.1
1.5 µm wafer	3.8 ± 0.1	3.4 ± 0.2	3.7 ± 0.1	1.4 ± 0.1
1.5 µm elastomer	3.7 ± 0.3	8.2 ± 0.2	17.6 ± 0.5	1.4 ± 0.10

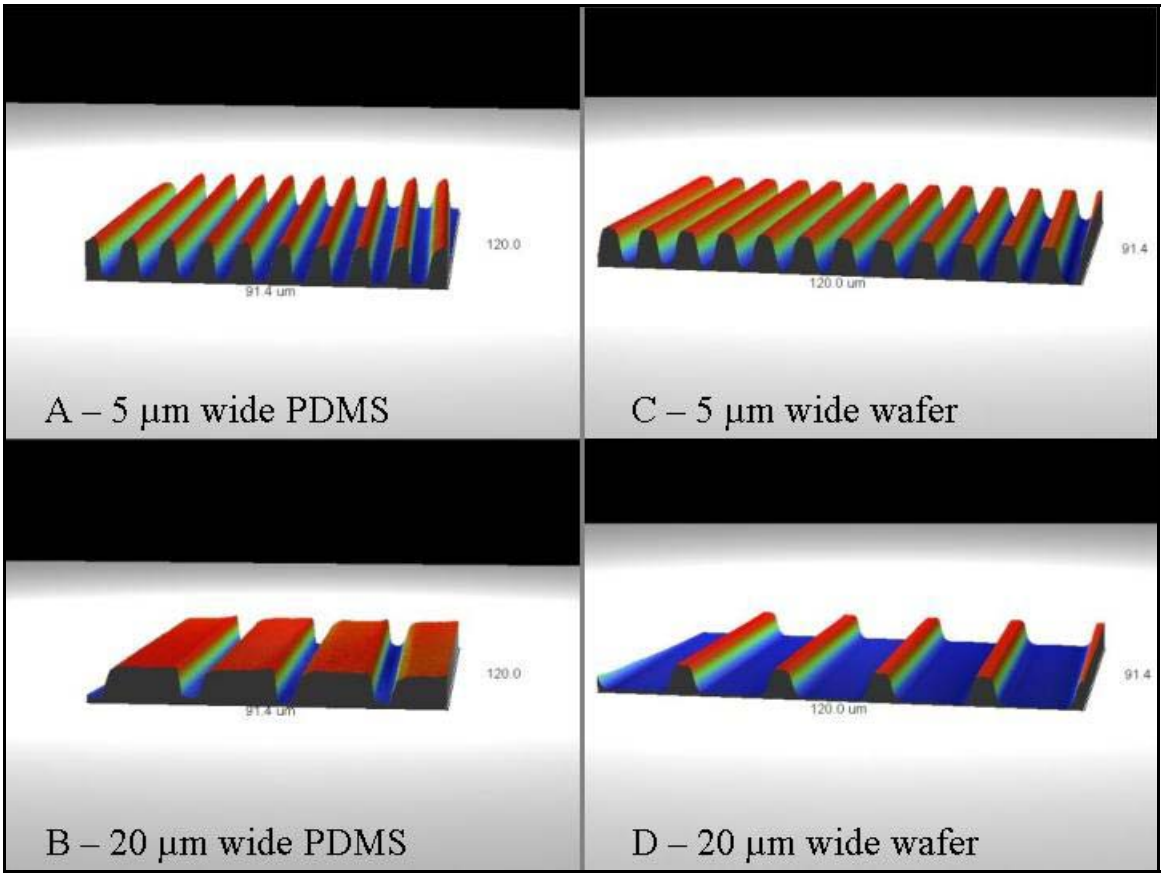

Figure 3.13 – 3-D images of 5% LMW elastomer copies (A, B) of a 1.5 µm wafer (C, D).

Some of the limitations of the optical profilometer system are a result of the scale and arrangement of the features. As can be seen by comparison of Figure 3.11 and Figure 3.12, both have similar shapes of ridges, with the sidewalls sloping downward so that the walls appear to not be vertical. Since the profilometer is non-contact and requires the reflectance of light, as the features get deeper and closer together, some data can be lost if the magnification is not high enough or if the material does not reflect light out of small features. For spacing greater than 5 μm, and magnifications of 50X or more, this problem is not as great. This instrument is a good addition to the analytical capabilities of a researcher since it is easy and quick to use with little to no sample modification, and gives a quality replication of the image surface in three dimensions. With the analysis reported in this chapter, coupled with the background in contact guidance and cell growth, a better understanding of the factors and variables involved in the growth of cells on textured surfaces is possible.

CHAPTER 4
CONTACT GUIDANCE OF ENDOTHELIAL CELLS

Introduction

In the previous chapters of this thesis, the principles of contact guidance and the materials used for this study have been detailed. The final step of this project was to examine the contact guidance phenomenon on a novel system to determine the effects of elastic modulus on a surface's ability to direct cell growth. Contact guidance was quantified on a group of silicone elastomers with elastic modulus values varying almost 800% but with similar surface energies. Textured surfaces made from four elastomer formulations were seeded with porcine vascular endothelial cells (PVECs). Cell nuclei were imaged and the nuclear shape was compared for surfaces of varying ridge dimension, groove depth, and material modulus.

Materials

Elastomer Substrates

As described in the previous chapter, the unmodified base elastomer is the *Silastic*® T-2 Silicone Moldmaking Rubber produced by Dow Corning. Three vinyl terminated PDMS based oligomers were included to give the elastic modulus a range from 0.3 MPa to 2.3 MPa. Pertinent information about the elastomer systems, including modulus and surface free energy, γ_s, is listed in Table 4.1. The vinyl-terminated oligomers were selected over non-functionalized oils due to their incorporation into the network structure and to minimize additive release.

Table 4.1 – Properties of elastomeric substrates for contact guidance experiments

Sample Reference	Additive	Modulus (MPa)	γ_s (mN/m)
Unmodified	None	1.4 ± 0.1	18.9
5% LMW	5% Vinyl terminated PDMS 550 g/mol	2.3 ± 0.5	19.1
5% HMW	5% Vinyl terminated PDMS 28,000 g/mol	1.0 ± 0.1	21.0
15% vinyl tris	15% Vinyltris-(trimethylsiloxy)silane	0.3 ± 0.1	17.1

Cell Culture and Seeding

Bovine plasma fibronectin was received as a lyophilized powder from Sigma (cat# F-4759, 2 mg). PVECs were obtained from Dr. Edward Block's lab at the Malcom Randall VAMC in Gainesville. Endothelial cells were obtained from the main pulmonary artery of 6 to 7 month old pigs and were propagated in monolayer cultures and characterized as described by Patel et al.[126] Third to sixth-passage cells in postconfluent monolayers maintained in RPMI 1640 medium (Life Technologies, Grand Island, NY) containing antibiotics (100 U/ml of penicillin, 100 µg/ml of streptomycin, 20 µg/ml of gentamicin, and 2 µg/ml of Fungizone) were used in all studies. Fetal bovine serum (FBS, was added at a 10% concentration for plating and growth. Falcon tissue culture flasks and 24 well plates were used for cell passaging and seeding. Trypsin/EDTA 1X solution was stored in frozen 10 mL aliquots. Hank's balanced salt solution (BSS) was used for washing flasks and samples. PVEC nuclei were stained with Hematoxylin 2 from Richard Allan Scientific. Cytoplasm and various features were stained with a 1% aqueous crystal violet solution.

Methods

Elastomer Sample Preparation

Silicone elastomer samples were prepared as described in the previous chapter. The four elastomer formulations reported in Table 4.1 were used for this portion of the study. Cure times and curing agent amounts are listed in the previous chapter, Table 3.3. For all samples, constant thickness was maintained at 3 mm with the use of appropriate spacers between glass plates. Textured sample were cast directly off silicon wafers with the patterns etched into the surface. Untextured films were cast between two PET sheets attached to glass plates. Samples were cut out using a punch with an interior diameter of 14.37 mm and outer diameter of 15.53 mm. All samples were sterilized in the same fashion by rinsing with 70% EtOH and drying overnight in a sterile hood.

Surface Treatment by Fibronectin

Some surfaces were coated with fibronectin (FN) as described in the previous chapter. Sterilized samples were placed in a 16 mm diameter well of a 24 well placte, and a 50 μg/mL solution of FN was added in 0.5 mL aliquots to each well with a sample. After exposure to vacuum to remove trapped air, samples were left to incubate for 1 hour at room temperature. The FN solution was aspirated out and then the samples were washed 3X with Hank's BSS.

Surface Treatment by RFGD Plasma

Textured surfaces were exposed to an argon RFGD plasma at 50 W for 5 minutes as described in the previous chapter after sterilization by EtOH. The argon regulator was set at 20 psi and the flowrate was 200 sccm. Samples were treated 4 at a time, 5.5 cm below the RF coils, with one sample from each material per treatment to ensure similar surface modification between batches. After treatment, the samples were moved to a

sterile hood and left exposed to air for 10 minutes for each sample, then transferred to a 24 well plate.

Cell Culture Techniques

PVECs were supplied by Bert Herrara from Dr. Edward Block's lab weekly as suspensions in 12 mL of media. All cells received from Dr. Block's lab were between passage 2 and 5. Cells were expanded by diluting the suspension to 20 mL with fresh media and subsequently transferred as 10 mL aliquots to a 75 cm^2 angled neck, vented tissue culture flask. Flasks were incubated at 37°C and 5% CO_2 for 48 hours, and then existing media was exchanged for fresh. Media was changed every 72 hours after that. Typically, the PVECs formed a confluent monolayer on the culture flask within 72 hours from initial plating.

Cell passage procedure

To passage the cells, confluent flasks were washed 3X with Hank's BSS. A few mL of trypsin/EDTA 1X solution was poured in the flask and swirled to counteract any remaining serum proteins and the remaining liquid was poured off. A small amount (~1-2 mL) of fresh trypsin/EDTA solution was added again, with just enough to coat the bottom of the flask. The flask was then placed in the incubator at 37°C for 5 minutes, and then checked with the inverted microscope to determine the appearance of the cells. Once the cells became rounded, the sides of the flasks were struck on each side to dislodge the remaining adherent cells. Serum containing media was added to counteract the trypsin, and the suspension was mixed by aspiration with a 10 mL pipet. The suspension was split into 3 flasks from each original flask and left to incubate as before.

Determination of cell suspension concentration

To determine the average amount of cells per mL in a cell suspension, a hemacytometer was used. A hemacytometer has a chamber with 10 separate grids each measuring 1 mm square. A coverslip was placed over the counting area, which resulted in a well 0.1 mm deep. Cell suspension was transferred by pipet to the edge of the coverslip, where the suspension was drawn into the chamber. Counts of 10 different squares were made, and the average count was multiplied by 10^4 to determine the average cells per mL in the suspension. If necessary, suspensions were diluted to achieve a cell count between 1 x 10^5 cells/mL and 2 x 10^5 cells/mL before seeding on samples.

Cell Seeding on Samples

For all samples, 1 mL of cell suspension was seeded into a well. Each sample has approximately 2 cm^2 of surface area, and at a seeding density of 2 x 10^5 cells/mL, then approximately 1 x 10^5 cells/cm^2 was added to the sample. For fibronectin-coated surfaces, the cells were suspended in serum free media since the adhesion protein was already adsorbed on the surface. Cells were seeded in normal 10% FBS media on plasma treated and untreated surfaces.

After seeding, the samples were incubated at 37°C and 5% CO_2. After 48 hours, the media was changed to remove non-adherent cells and replace with fresh media. Plasma treated surfaces exhibited an initial period where endothelial cells clumped into groups (after 24 hours), and then eventually spread out to a monolayer. Cells on these surfaces were left to grow for 5 days. Fibronectin coated surfaces showed improved cell spreading and attachment, and cells were imaged after 48-72 hours.

Cell Staining and Image Capture

Many methods were examined to effectively stain the cells. To image the entire cell body and morphology, cells were stained in an aqueous 1% crystal violet solution. First, after removing the media, cells were washed 2X with BSS, then fixed with cold 10% n-buffered formalin for 20 minutes in the culture well. After removal of the formalin, fixed samples were washed with BSS and crystal violet was added and cells stained for 20 minutes. Samples were removed from the wells using a needle to minimize flexing the substrates. The samples were washed in saline and placed on a slide, then covered with a coverslip to prevent drying of the surface.

To image only the nucleus for the nuclear form factor, a hematoxylin stain was used. Hematoxylin stains nuclear materials, specifically basophilic structures such as DNA and RNA and was therefore chosen so that nuclear elongation could be used to quantify contact guidance. The method followed the Sigma method for Gill's hematoxylin staining. Briefly, cells were fixed in 95% EtOH for 10 minutes, rinsed 2X with tap water, and stained for 2 minutes in hematoxylin. Longer staining times increased the intensity of the nuclear stain, but also increased staining of the cytoplasm. After the hematoxylin, the samples were rinsed 2X in water and 2X in 95% EtOH. The substrates were placed on a slide and covered with a coverslip.

Cells were imaged on the surface at 200X using a Nikon Optiphot microscope and Matrox image capturing system. Multiple images were taken at each feature width that included at least 5 nuclei. Images were saved as a jpeg format and imported to Adobe Photoshop for analysis.

Image Analysis

Images were analyzed to measure the ratio of the length to the width of each nucleus. A schematic of the measurements taken can be found in Figure 4.1.

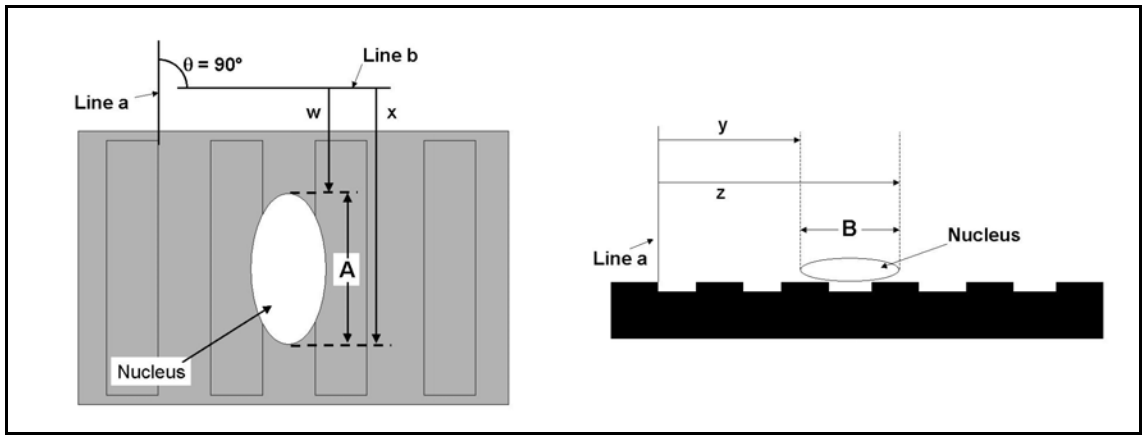

Figure 4.1 – Representation of the values measured in the nuclear form factor. The left side of the image is a top view of a nucleus on a microtextured substrate, while the right side is a cross-sectional view. The length measured is represented by A, while the width is represented by B. The nuclear form factor is Log (A/B) (Drawing by Chuck Seegert)

The imported image files were modified to improve the contrast between the nuclei and the background using Adobe Photoshop 6.0. A pictorial explanation of the steps can be found in Figure 4.2. All images were adjusted using the auto-contrast macro in the software package (Figure 4.2B). Then, batches of images were opened that came from the same sample since they all had the same angle of orientation. By drawing a measured line along the length of a groove, and then using the arbitrary rotate command, the image is automatically rotated by the same angle as the measured line. The end effect is to line up the ridges vertically on the computer screen (Figure 4.2C). By recording the commands and initiating a batch process over the range of the opened images, all of the features for each sample were aligned.

Image Processing Technique

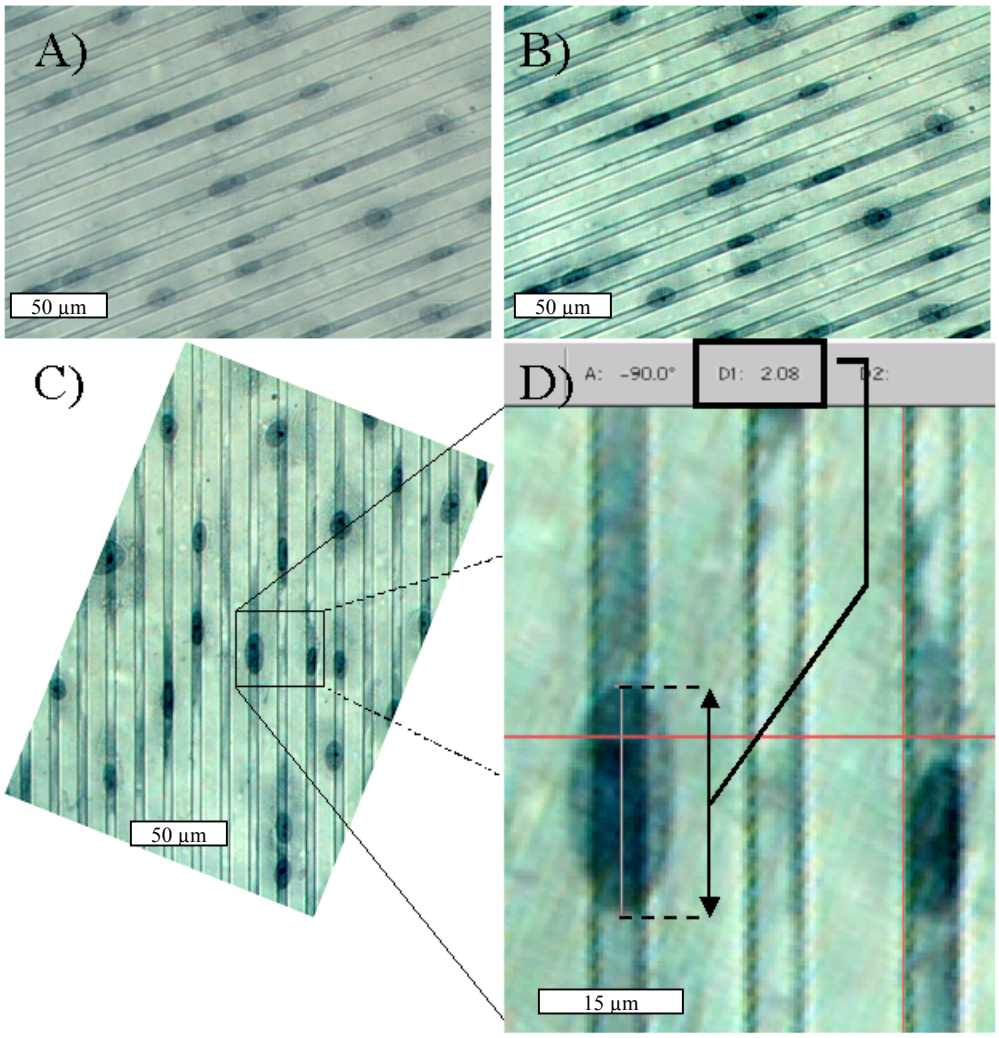

Figure 4.2 – Steps in image processing technique of hematoxylin stained nuclei. The original picture (A) is contrasted (B), rotated to align the textures (C), and then measured for length (D) and width (not shown). The reported value is log(Length/Width)

The benefit of the vertical alignment is to improve the efficiency of measuring the nuclei. The procedure introduced by Dunn and Heath[10] requires the measurement of the length and width of nucleus at its widest point, where the length measured is parallel to

the ridge, and the width is perpendicular. With the images aligned vertically, the measurement lines can be constrained by the software to perfectly vertical or horizontal, and so by using that method the maximum length and maximum width of each nucleus was measured and entered into an Excel spreadsheet. A 5 x 5 grid was superimposed on the images, and 5 nuclei were chosen per image, each from a separate square of the grid. Using this method, at least 20 nuclei per sample setting were quantified.

Results and Discussion

Contact Guidance on Textured Surfaces

As discussed in Chapter 2, surface ridges and grooves typically act to elongate cells along the ridge. This phenomenon is mainly reported in qualitative fashion, and fibroblasts are predominant as the cell system, since they are relatively easy to grow and have shown good results in terms of contact guidance. Quantitative studies of contact guidance on textured surfaces have used SEM and phase contrast microscopy to map the entire cell body and try to determine its alignment. A serious limitation to this method is the fact that unless the cells are isolated from others, the cellular dimensions and alignment can be difficult to determine. From personal experience, cells that are not in contact with others are typically more elongated and tend to show greater contact guidance than confluent cells. Other methods to quantify contact guidance stain actin filaments and other cytoskeleton components to detect the alignment of the interior stress fibers with fluorescent or confocal microscopy.

For cells in this study, groups of cells were examined, rather than individual cells apart from the rest of the culture. The main purpose of this project was to examine the effects of modulus as a factor involved in the ability of a substrate to direct cell growth.

While modifying the underlying substrate's mechanical properties might alter a cells ability to adhere and change its morphology, it will not direct cells to grow in a certain pattern. In order to affect this change, the surface was patterned with microtexture in the form of ridges, as characterized in the previous chapter.

Surface texture was examined using the unmodified elastomer as the reference material. For this portion of the experiment, two main factors were examined, ridge width and groove depth. As stated in the previous chapter, plasma treatment of the surface resulted in small random cracks and an unreliable texture dimension. Due to the concerns as to the effects of the plasma treatment to the fidelity of textures, fibronectin adsorbed materials were examined most closely. Figure 4.3 is a main effects plot of fibronectin coated unmodified elastomer. The average of all the data points is represented by the dotted line, and the individual means are compared to this overall mean. The term "Feature" in the graphs and subsequent analysis refers to the width in microns of the ridges in the section examined. All of the grooves were 5 μm in width. The term "depth" refers to the depth of the grooves in microns, either 1.5 μm or 5 μm. Smooth images were taken from the same samples, at least 50 μm from the closest texture.

Log (L/W) is defined as the nuclear form factor and is the variable that measures the strength of nuclei alignment along the ridges. The more positive this variable is, the more the nuclei exhibit contact guidance. Values greater than 0.15-0.20 are typically very well aligned. The closer log (L/W) is to zero, the less the cell shows deference to the topography at all. A negative number implies that the cells are guided orthogonal to the textures.

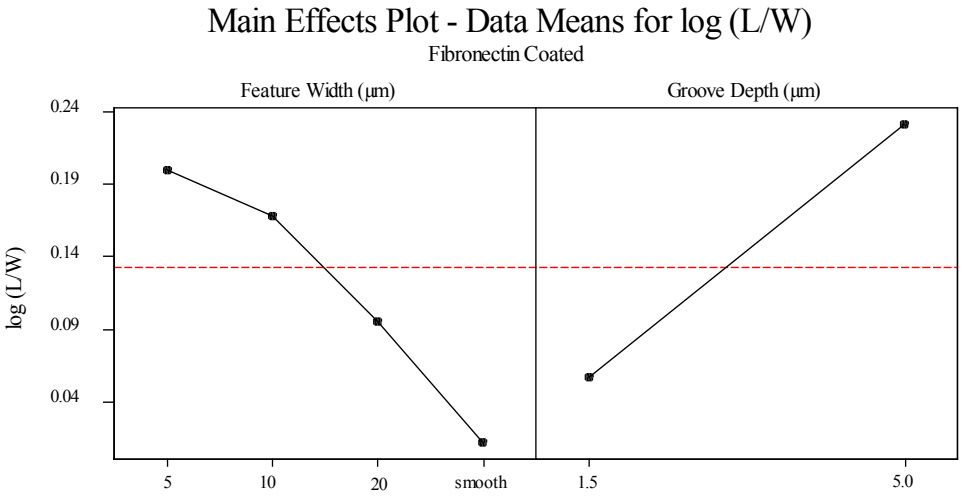

Figure 4.3 – Main Effects Plot of the data means of fibronectin coated unmodified elastomers at various ridge widths (Feature) and groove depths (Depth)

The main effects plot helps to elucidate which factors and levels play a role in the system. The more the data changes between levels, the greater the effect. Figure 4.4 is an interaction plot generated by Minitab that demonstrates the changes at the different factor levels for fibronectin coated unmodified elastomer. The important point that is illustrated here is that at the deeper groove depths, the greater the alignment of the nuclei to the ridges. One-way analysis of variance (ANOVA) and a multiple comparison test (Tukey, 95% CI) on each depth comparing the different feature widths demonstrate a significant difference between each level at the 5 µm depth, but only a statistical difference at 1.5 µm between 5 µm wide ridges and smooth textures. One of the difficulties in the analysis of these samples is in the fact that for the smooth samples, the nuclei are not round, but elongated in random directions. The effect of this is to give a

mean value for log (L/W) for the smooth areas around zero, but with a large standard deviation.

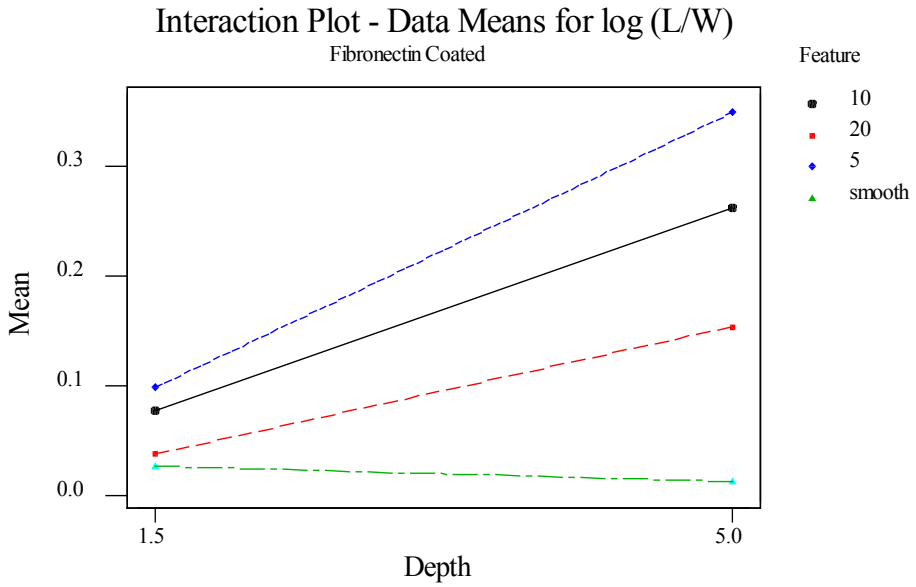

Figure 4.4 – Interaction plot representing the change in contact guidance with depth and feature width for fibronectin coated silicone elastomer.

Figure 4.5 and Figure 4.6 are main effects and interaction plots for plasma treated unmodified elastomers generated by Minitab. These are the same plots as Figure 4.3 and Figure 4.4, which are treated with FN. As can be seen in Figure 4.5, the difference between the feature widths is not as obvious, and the effect of the depth on the alignment does not play as large a role from 1.5 μm to 5 μm, as confirmed by the small slope.

A two-way ANOVA comparison on plasma treated unmodified elastomer comparing the effects of feature size and depth show that when including the smooth areas in the analysis, the feature size is a very significant contributor to variance ($p < 0.0001$) while depth is not a significant influence. By removing the smooth terms and

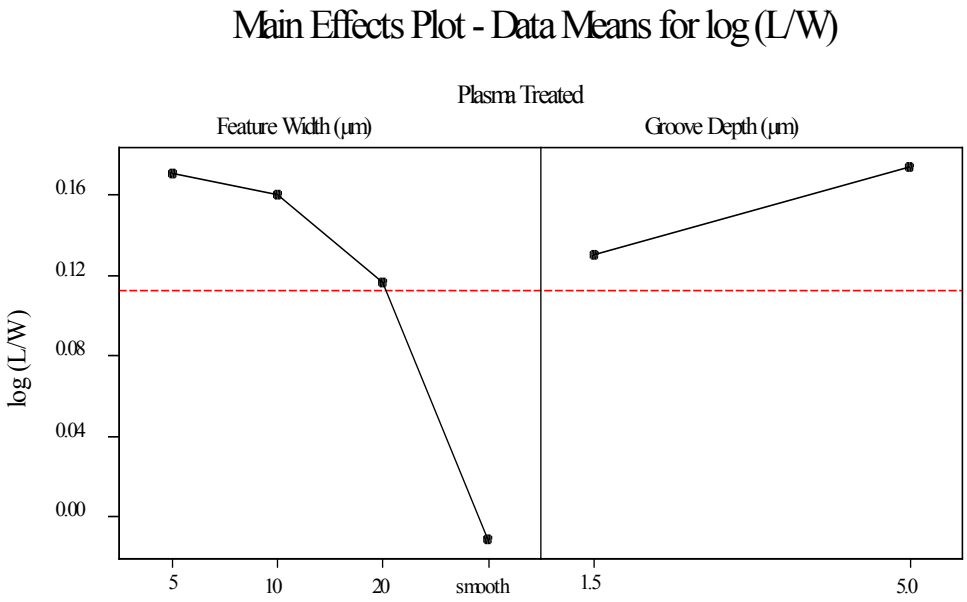

Figure 4.5 – Main Effects Plot of the data means for plasma treated unmodified elastomers. The left side of the plot compares effects due to the feature width, while the right side compares the groove depth.

repeating the analysis such that the comparison is strictly on the textured surfaces, both the width and the depth are significant sources of variance ($p < 0.05$).

One way ANOVA comparisons followed by a multi-comparison test (Tukey, 95% CI) between the ridge widths at constant depth on plasma treated unmodified elastomer show that for each width there is a significant difference when compared to smooth samples, but the difference is not significant when compared to the other widths. To put it simply, for plasma treated samples at both depths, each groove width shows significantly more alignment when compared to a smooth surface, but there is no statistical difference when comparing the different permutations of the three ridge widths.

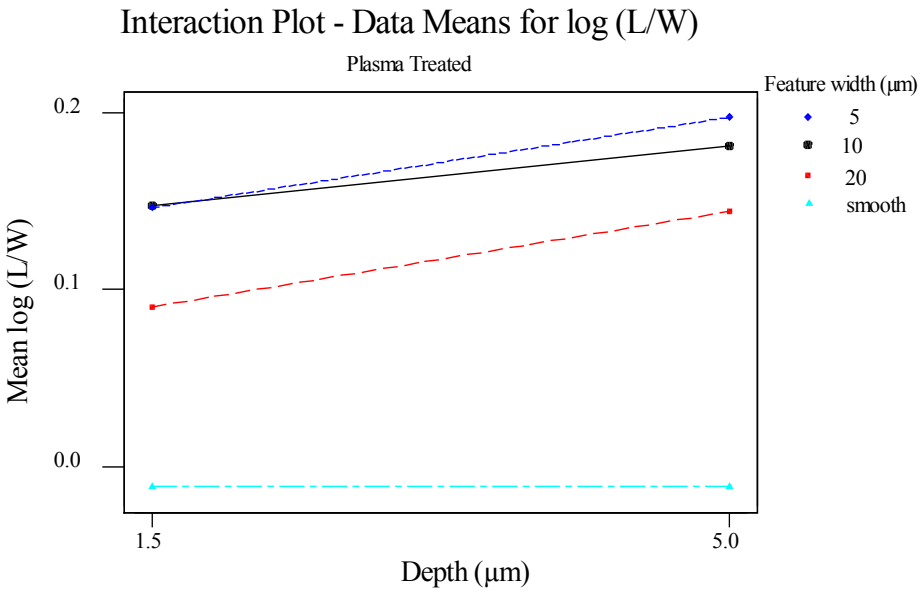

Figure 4.6 – Interaction plot representing the change in contact guidance with depth and feature width for plasma treated silicone elastomer.

In this graph the contact guidance data for PVECs grown on the neat sample with no surface modification at 1.5 µm depth is included. Due to substrate production limitations at the 5 µm depth, untreated samples were not available for analysis.

In comparing these results to the fibronectin coated surfaces, one point that stands out is that for the 1.5 µm deep FN coated substrates only the 5 µm wide ridges were significantly different from the untextured surfaces, while at 5 µm there was a statistically significant (alpha = 0.05) higher degree of alignment. The 1.5 µm plasma treated surfaces did have significant alignment compared to smooth surfaces, and a higher log (L/W) value than 1.5 µm fibronectin samples. However, due to the surface irregularities of the plasma treated surface explained in the previous chapter and the fact that a silica-like layer would expose the cell to a seemingly harder substrate; direct

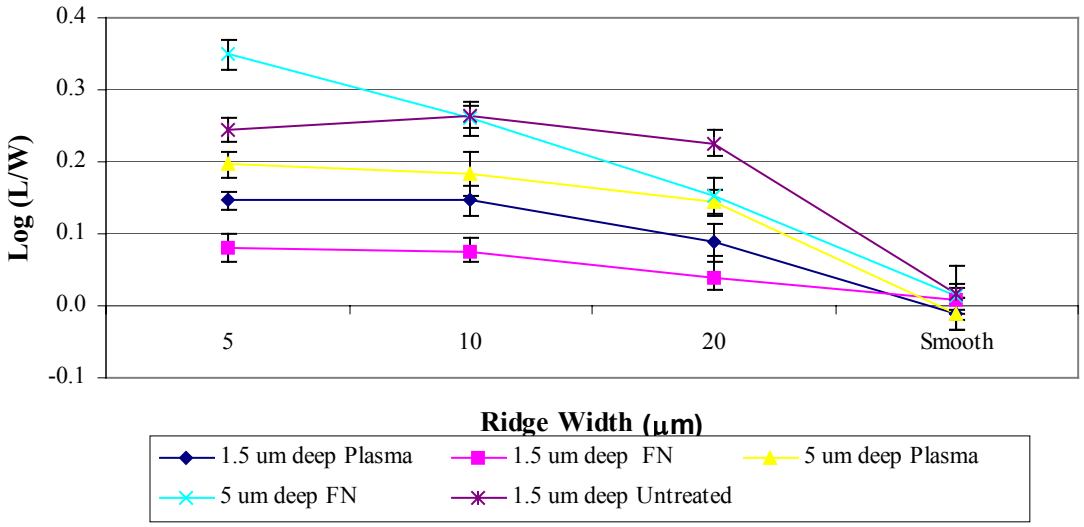

Figure 4.7 – Comparison of surface treatments on textured unmodified silicone elastomer by ridge width and groove depth (error bars represent standard error of mean)

comparison of the two methods may not be appropriate due to material differences. The untreated samples show a high degree of alignment at all texture settings. Cell attachment and proliferation on these surfaces was significantly lower than on the treated surfaces, but those cells that were attached were aligned at all levels of texture. The morphology of these cells was highly elongated (compare Figure 4.8 and Figure 4.9) as the cells attempted spread and stabilize. The fact that almost all of the cells showed a high degree of alignment on the untreated surface suggests that when they come into contact with a surface with less than ideal adhesion capability, the presence of surface texture plays an increasingly important role.

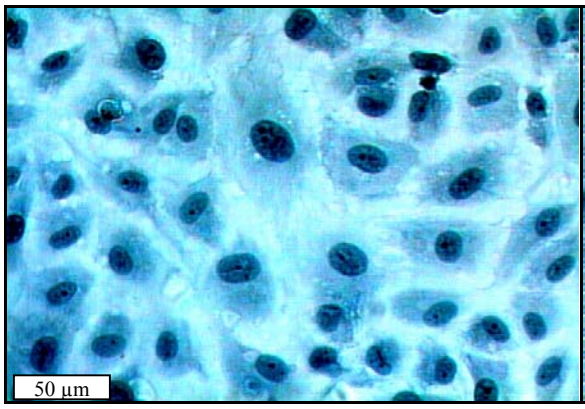

Figure 4.8 – PVECs grown on untextured fibronectin coated LMW sample stained with hematoxylin

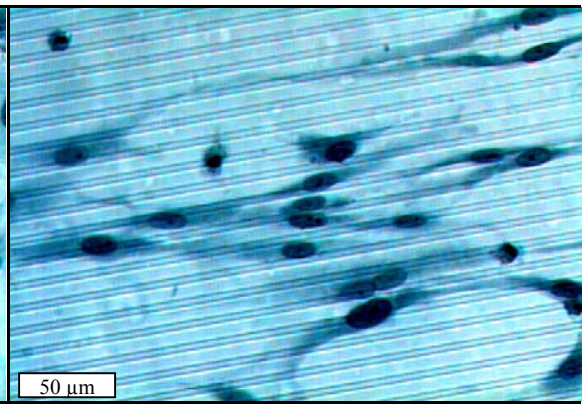

Figure 4.9 – PVECs grown on 5 µm spacing 1.5 µm deep untreated LMW stained with hematoxylin

Contact Guidance on Textured Surfaces of Varying Modulus

The main unknown factor in the design of this project is the modulus of the material and its effect on contact guidance. As discussed in Chapter 2, many different materials, from metals to elastomers, have been examined in the study of direct cell growth. In published research on contact guidance, the modulus of the sample substrate is very rarely reported. Most materials used with different mechanical properties have also significantly different surface energetics, which directly affects protein adsorption and adhesion, making a comparison due to modulus improbable. These effects would more than likely wash out any change due to the effects of mechanical properties. The purpose of this section is to examine whether or not the modulus, as a measure of the compliance, can significantly affect the ability of a material to direct cell growth in the range covered by these materials.

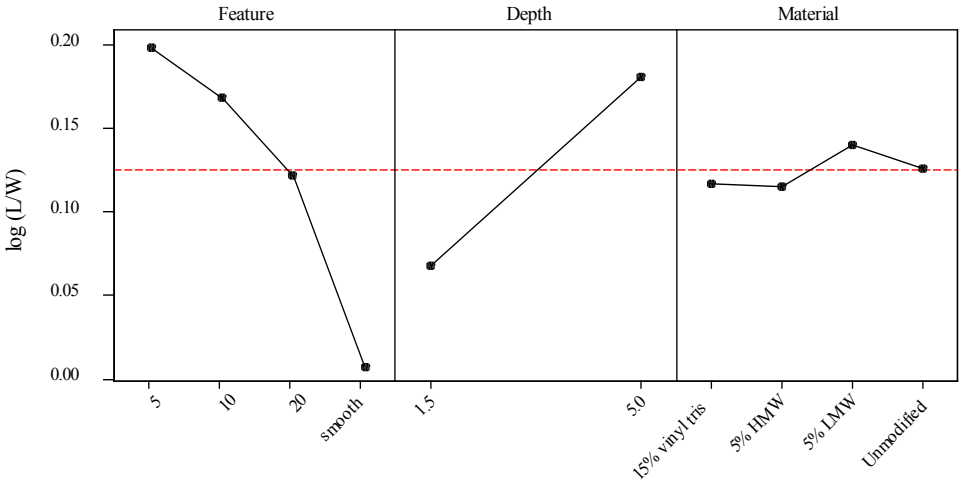

Figure 4.10 – Main effects plot comparing log (L/W) to feature width, feature depth, and material used on fibronectin-coated elastomers.

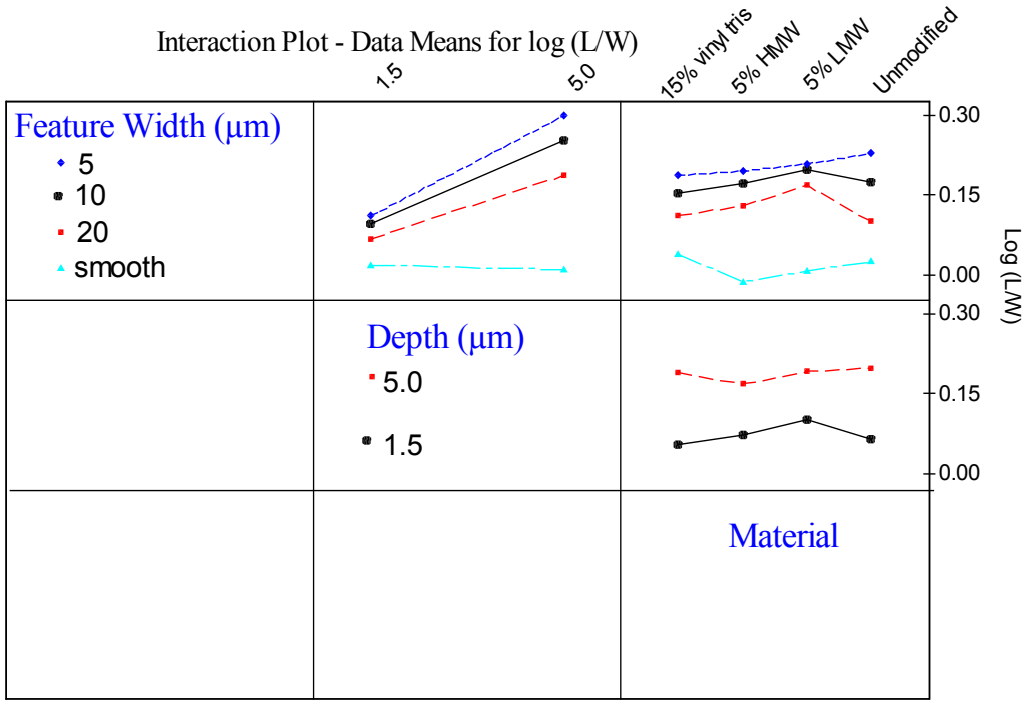

Figure 4.11 – Interaction plot representing the change in factors of PVECs grown on fibronectin coated materials.

Figure 4.10 is a main effects plot from Minitab similar to Figure 4.3 and Figure 4.5 on fibronectin-coated surfaces. As mentioned previously, due to the uncertainties with the reproducibility of plasma treated surfaces, fibronectin materials will mainly be examined. As seen before, the effects of depth and width of ridges seem to play the largest role in the response of log (L/W). The relative flatness of the material interaction implies that there is little contribution due to a change in modulus. In qualitatively interpreting Figure 4.10 and Figure 4.11, it appears that contact guidance increases with decreasing feature width and increasing depth on each of the materials, but a direct correlation between the material choice and the degree of alignment is not obvious. One way ANOVA comparisons followed by a Tukey multi-comparison test (CI = 0.95) for the 5 μm depth materials show no significant difference between any of the materials at the 5 μm groove width. It is apparent from Figure 4.12 that the groove depth at that point is much more significant and few trends can be found in relating the modulus. In effect, the groove depth is overpowering any effect that modulus might have on the contact guidance.

At the 1.5 μm depth, there are more significant differences with respect to materials. At the 5 μm and 10 μm ridge width, there is a significant difference between the 5% LMW material and the 15% vinyl tris material with respect to log (L/W). The 1.5 μm data is represented in Figure 4.13.

Note that as reported in Table 4.1, these represent the high modulus (2.34 MPa) and low modulus (0.3 MPa) materials respectively. At 20 μm ridge widths, there is no significant difference between the two. Figure 4.14 compares the effect of ridge width and groove depth strictly on the LMW and Tris surfaces. The trend of the materials is to

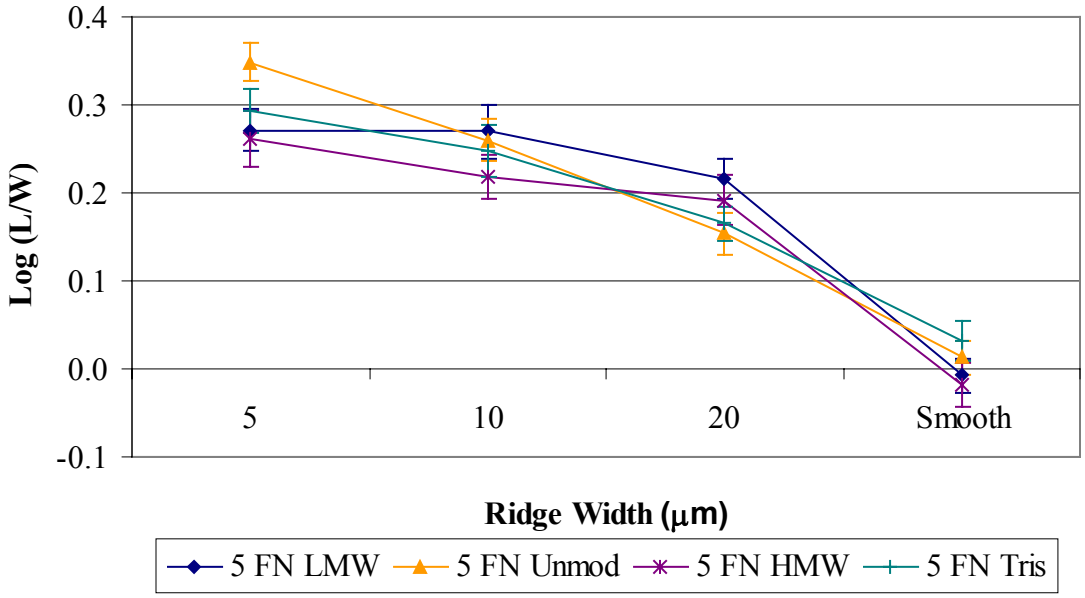

Figure 4.12 – Comparison of materials on textured unmodified silicone elastomer by ridge width on 5 µm deep grooves (error bars represent s.e.m.)

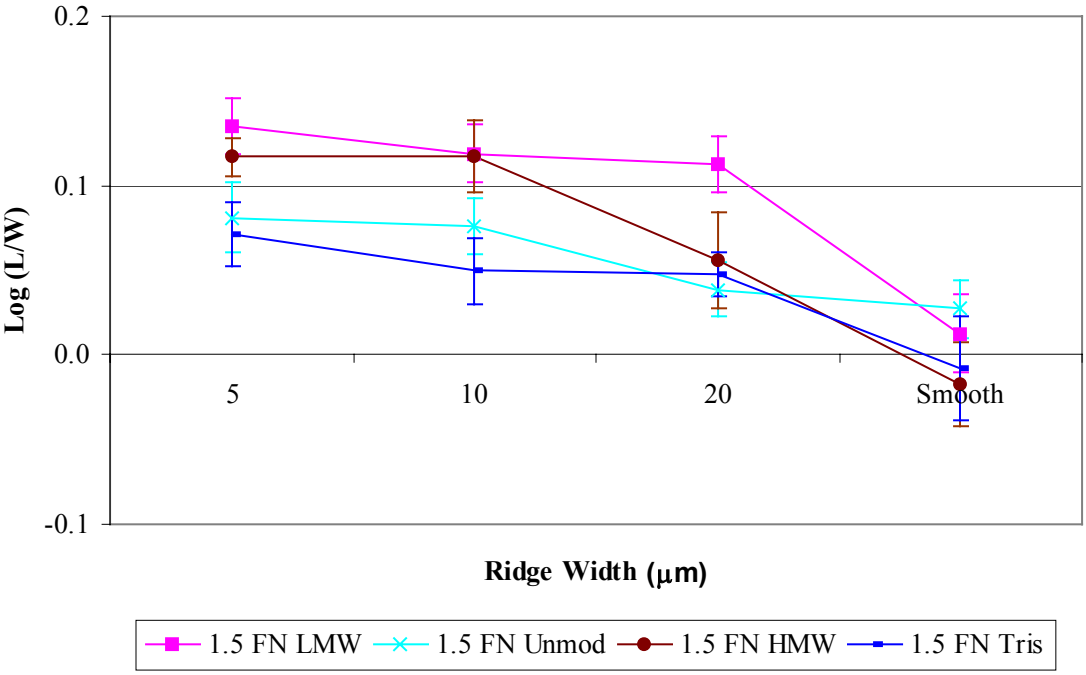

Figure 4.13 – Comparison of materials on textured unmodified silicone elastomer by ridge width on 5 µm deep grooves (error bars represent s.e.m.)

show increased contact guidance on the high modulus material. As stated before, this effect is not significant in the deeper grooves, and at 5 μm the low modulus tris sample even shows higher contact guidance, albeit statistically insignificant.

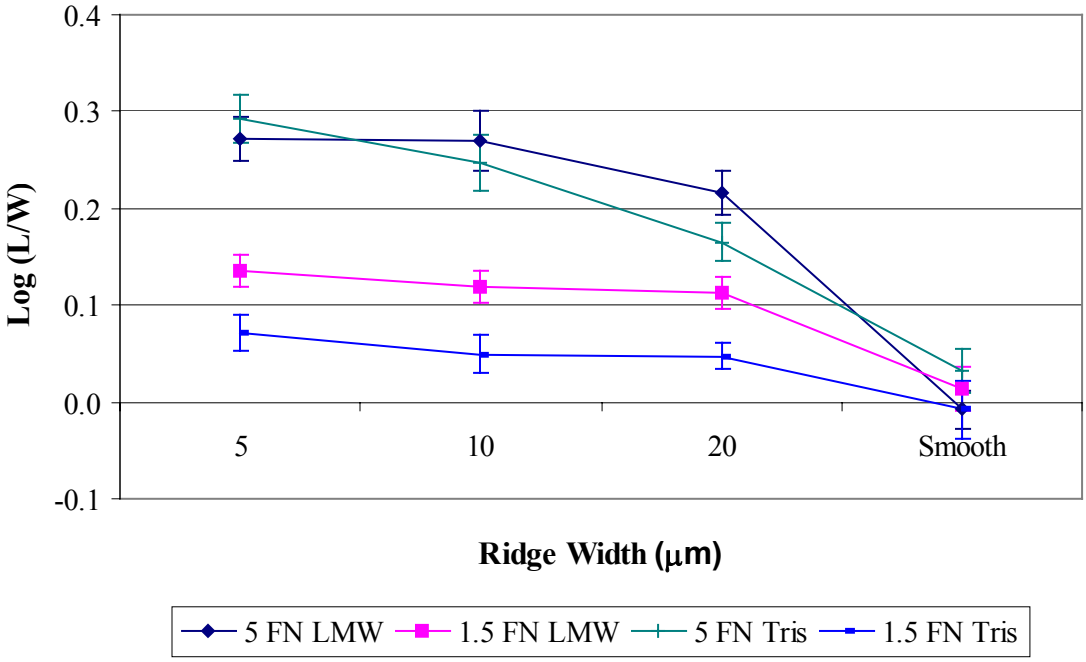

Figure 4.14 – Comparison of ridge width and groove depth to the high modulus material (LMW) and the low modulus material (Tris) – (error bars represent s.e.m.)

Since the 5 μm deep grooves have shown the strongest factors for contact guidance, the reason there is not a significant difference between materials at the greater depth might be that the importance of the groove depth overpowers any change due to the modulus. At the lower depth where the effect of the depth is not as great, it appears that the modulus of the surface alters its ability to direct the growth of cells. According to the data and trends, the higher modulus material seems to enhance the contact guidance phenomenon.

As discussed in Chapter 2, cells attach to surfaces at focal adhesions, and they impart a stress upon the substrate which is balanced by the material and acts as a counterweight so to speak improving adhesion. Researchers have examined the forces of cells such as fibroblasts on elastomeric substrates, using low modulus (~ 15 kPa) silicone films to quantify the forces of adhesion.[87] These cells continually pull and contract against these surfaces until they reach a balance, the equivalent of pulling the slack out of a rope until it is taut. Fibroblastic cells on higher modulus materials were shown to spread better and were of a more constant shape, while cells on lower modulus materials were more active and elongated.[98]

Possibly the cells elongate along the grooves because they can pull along the length of the groove as opposed to the width, which is more compliant due to its reduced thickness. Since they have more resistance along the length, they have a more stable opposing force to pull and align to. At higher ridge widths, this effect is lessened by the increased continuous surface area for attachment as well as possibly the increased thickness of the ridge. In this study, vascular endothelial cells were shown to preferentially align along the length of a groove and increased that alignment as the groove depth increased. The fact that changing the modulus had little effect on the alignment for the deeper grooves is not completely unexpected, since it is well documented that groove depth plays an important role in contact guidance, while the contribution due to the mechanical properties is not well defined or studied. However, if mechanical stability is a main factor in directing the cell growth, then one should see a greater effect on the deeper features, since the ridges are even less mechanically stable at the higher aspect ratio. Another issue is that at deeper groove widths, the cells are more

likely to span a groove without touching the bottom of the groove. This in effect lines up the possible areas of focal adhesions by leaving the only area for adhesion on the top of the ridge.

At lower groove widths and shallower grooves, the modulus of the material seems to play a more important role, but one only seen by comparing the highest and lowest modulus silicone materials available. Substrates like titanium and polystyrene could be used as well for comparison as a much higher modulus material, but their behavior in regards to surface energy will play a significant role that cannot be overlooked.

The nuclear form factor is a useful tool for elucidating the alignment of a cell, and one that may in the future become more widely used. The power of the model stems from the ease in imaging and data processing as compared to examining strictly actin filaments or trying to map an entire cell.[2, 37] The flaws in its use come from its sensitivity to less elongated cells and in comparing cells that are aligned at 45° angle to those with nuclei that are more rounded. Both types of nuclei would give similar results of zero using the nuclear form factor. While neither are aligned to the features, a group of cells aligned at 45° would result in an interpretation that the cells were not aligned or randomly aligned, when in fact they could be aligned all in one direction at 45° due to some other unknown factor. In reference to sensitivity, a simple model comparison can show one of the drawbacks of using the nuclear form factor. A highly elongated nucleus oriented 30° to the direction of the features can have the same dimensions in length and width as a nucleus that is perfectly aligned to the features, but not as elongated. With a large sample size, these problems can be minimized, but they should be issues to consider for potential researchers. By incorporating a corroborating measurement such as the

angle of deflection of the nuclei's long axis from the direction of the ridges, or combining cystoskeletal measurements, more confidence in the method would be assured for future studies and solve both of these issues.

CHAPTER 5
CONCLUSIONS AND FUTURE WORK

Conclusions

Microtextured Surfaces

To examine the effects of contact guidance on silicone elastomers, microtextured substrates were produced with reproducible and well-defined surfaces. Ridges of 10,000 μm length were fabricated at 3 different widths: 5 μm, 10 μm, and 20 μm, separated by 5 μm wide grooves to determine the effect of separation of features on the alignment of porcine vascular endothelial cells. Two depths were examined: 5 μm and 1.5 μm. The silicone elastomer samples were produced by casting a film on a textured mold and allowing the samples to cure. Molds used were either silicon wafers or epoxy replicates of the wafers. The surfaces were created with micromachining technology, specifically photolithographic patterning followed by reactive ion etching. After examination of the surfaces by optical profilometry, it was determined that the silicone copies faithfully reproduced the textured surface and the textures were of the expected design. Closer examination demonstrated that the 1.5 μm deep wafer and samples had a more rounded appearance and had ridge widths ~1 μm less than expected. The depths measured corresponded with designed values of 1.5 μm and 5 μm within experimental error. All elastomer types used in this study faithfully reproduced the applied texture and gave a stable substrate for comparison.

Surface Energy and Treatment

Elastomer samples were examined with contact angles to determine their relative wettability and surface free energy. Formulations of elastomer with both functionalized and non-functionalized PDMS oligomer additives were examined, and there was no significant effect to the surface energy as determined by Zisman plots using 5 separate liquids. Sessile drop contact angles measured with a goniometer were measured, and the surface energy of the unmodified elastomer samples was found to be 18.9 mN/m. Water contact angles were typically ~ 110° for unmodified samples.

Surfaces were treated with fibronectin and radiofrequency glow discharge plasma in argon for 5 minutes at 50 W. Both treatments significantly increased the hydrophilicity after treatment, as measured by captive bubble contact angles, from 86.7° ± 4.3° for the unmodified sample to 14.5° ± 3.5° for fibronectin adsorbed surfaces and < 10° for RFGD plasma treated surfaces. Dynamic contact angle analysis was performed on the unmodified elastomer and materials with non-functional PDMS oligomers added. Advancing contact angles varied between 100.5° and 115.1° and the hysteresis between the advancing and receding angles was between 35° - 45° except for high molecular weight, high weight percent additive which formed a visible layer of oil on the surface. The hysteresis on this surface was quite low (11.6° ± 4.4°). Dynamic contact angle analysis of textured surfaces showed a difference in smooth and textured areas, although quantitative data was not available due to experimental uncertainty. The trend of the graphs demonstrated an increase in observed advancing water contact angles, which is possibly due to composite surfaces with air trapped in the textures.

Analysis of the RFGD treated PDMS elastomer surfaces revealed defects that were caused by the plasma treatment. Groove depths decreased by 40% in some cases as

the material was ablated by the plasma. Cracks on the order of 0.5-1.5 μm were seen to form after mechanical manipulation of treated surfaces. This phenomenon seems to be a result of the cracking of a hard silica-like layer on the surface.[116] Due to the uncertainties with the feature dimensions and surface mechanical properties, fibronectin adsorbed surfaces were used for the main analysis of the effects of contact guidance.

Contact Guidance on Textured Elastomers

Contact guidance of PVECs on textured silicone elastomers was measured by the nuclear form factor, in which the log of the ratio of nuclear length to width was presented. Results demonstrated that as the ridge width decreased from 20 μm to 5 μm contact guidance increased, as well as when the depth of the grooves increased from 1.5 μm to 5 μm. Data analysis showed that the groove depth was the most important factor in nuclear alignment. Average values of the nuclear form factor for 5 μm deep, 5 μm wide samples exceeded 0.3, which implies the length was more than twice the width on average. Shallower grooves increased the length of the nuclei by approximately 25% in comparison to the width.

Contact guidance on fibronectin-coated elastomers was examined to determine the effect of modulus. It was expected that higher modulus materials would increase the effect of contact guidance. Elastic modulus on 4 elastomers was measured by tensile tests and resulted in a range of values from 0.3 MPa to 2.34 MPa. There was no significant difference in the contact guidance on the deep 5 μm grooves with varying modulus. The 1.5 μm deep grooves showed a significant increase in the alignment of cells to the groove in the highest modulus material compared to the lowest modulus material for the 5 μm and 10 μm wide ridges. The conclusion to be taken from this data is that modulus does seem to play a role in the determination of contact guidance, but

other factors such as groove width and especially depth are more significant. With this knowledge, and with future work, ideal values to fine tune materials may be possible to direct and control cell growth.

Future Work

The importance of controlling cell growth and behavior cannot be underestimated and the phenomenon of contact guidance is only recently approaching maturity. Several areas for future study and improvement are possible and are listed below.

Surface Treatment

- Optimization of plasma treatment needs to be examined, as well as the reasons for the unwanted effects. Argon RFGD at 50 W for 5 minutes is a standard treatment in the literature, and the reasons for the deviations should be investigated.
- Tether adhesion molecules to silicone surfaces to examine modulus affects with a permanently bound treatment.

Topographical Design

- Smaller ridge widths and an intermediate groove depth should be examined since the data shows that smaller ridge widths improve contact guidance, but the deeper groove depths mask the effect of modulus.
- Ridge widths on the order of 0.5 μm, 1 μm, and 2.5 μm would give useful data as to the limits of the ridge effect.
- Opposite or “negative” designs of the current elastomers would be useful in seeing the effect of a constant 5 μm ridge separated by varying smooth areas.

Cell Studies

- Examination of tissue growth from a central area to uncovered textured substrates should be relatively easy to set up and characterize.
- Growth patterns of endothelial cells along a textured interior surface of a cylinder would more closely model a seeded vascular graft response.

LIST OF REFERENCES

1. Curtis, A.S.G. and P. Clark. The effects of topographic and mechanical properties of materials on cell behavior. *Critical Reviews in Biocompatibility*, 1990. **5**(4): p. 343-362.

2. Curtis, A.S.G. and C.D.W. Wilkinson. Review: Topographical control of cells. *Biomaterials*, 1997. **18**: p. 1573-1583.

3. Bhatia, S.N. and C.S. Chen. Tissue Engineering at the Micro-Scale. *Biomedical Microdevices*, 1999. **2**(2): p. 131-144.

4. Brady, R.F. and I.L. Singer. Mechanical Factors Favoring Release from Fouling Release Coatings. *Biofouling*, 2000. **15**(1-3): p. 73-81.

5. Singer, I.L., J.G. Kohl, and M. Patterson. Mechanical Aspects of Silicone Coatings for Hard Foulant Control. *Biofouling*, 2000. **16**(2-4): p. 301-309.

6. Weiss, P. *In vitro* experiments on the factors determining the course of the outgrowing nerve fiber. *The Journal of Experimental Zoology*, 1934. **69**: p. 393.

7. Weiss, P. Experiments on cell and axon orientation in vitro: the role of colloidal exudates in tissue organization. *The Journal of Experimental Zoology*, 1945. **100**: p. 353.

8. Harrison, R.G. On the stereotropism of embryonic cells. *Science*, 1911. **34**: p. 279.

9. Rovensky, Y.A., I.L. Slavnaja, and J.M. Vasiliev. Behaviour of fibroblast-like cells on grooved surfaces. *Experimental Cell Research*, 1971. **65**: p. 193-201.

10. Dunn, G.A. and J.P. Heath. A new hypothesis of contact guidance in tissue cells. *Experimental Cell Research*, 1976. **101**: p. 1-14.

11. den Braber, E.T., J.E. de Ruijter, H.T.J. Smits, L.A. Ginsel, A.F. von Recum, and J.A. Jansen. Effect of parallel surface microgrooves and surface energy on cell growth. *Journal of Biomedical Materials Research*, 1995. **29**(4): p. 511-518.

12. den Braber, E.T., J.E. de Ruijter, H.T.J. Smits, L.A. Ginsel, A.F. von Recum, and J.A. Jansen. Quantitative analysis of fibroblast morphology on microgrooved surfaces with various groove and ridge dimensions. *Biomaterials*, 1996. **17**(21): p. 2037-2044.

13. Mudera, V.C., R. Pleass, M. Eastwood, R. Tarnuzzer, G. Schultz, P. Khaw, D.A. McGrouther, and R.A. Brown. Molecular Responses of Human Dermal Fibroblasts to Dual Cues: Contact Guidance and Mechanical Load. *Cell Motility and the Cytoskeleton*, 2000. **45**: p. 1-9.

14. van Kooten, T.G. and A.F. von Recum. Cell Adhesion to Textured Silicone Surfaces: The Influence of Time of Adhesion and Texture on Focal Contact and Fibronectin Fibril Formation. *Tissue Engineering*, 1999. **5**(3): p. 223-240.

15. Walboomers, X.F., H.J.E. Croes, L.A. Ginsel, and J.A. Jansen. Contact guidance of rat fibroblasts on various implant materials. *Journal of Biomedical Materials Research*, 1999. **47**: p. 204-212.

16. Clark, P., P. Connolly, A.S.G. Curtis, J.A.T. Dow, and C.D.W. Wilkinson. Topographical control of cell behaviour: I. Simple step cues. *Development*, 1987. **99**: p. 439-448.

17. Clark, P., P. Connolly, A.S.G. Curtis, J.A.T. Dow, and C.D.W. Wilkinson. Topographical control of cell behaviour: II. multiple grooved substrata. *Development*, 1990. **108**: p. 635-644.

18. Matsuzaka, K., X.F. Walboomers, J.E. de Ruijter, and J.A. Jansen. The effect of poly-L-lactic acid with parallel surface micro groove on osteoblast-like cells in vitro. *Biomaterials*, 1999. **20**: p. 1293-1301.

19. Schmidt, J.A. and A.F. von Recum. Macrophage response to microtextured silicone. *Biomaterials*, 1992. **13**(15): p. 1059-1069.

20. Wojciak-Stothard, B., A.S.G. Curtis, W. Monaghan, K. Macdonald, and C.D. Wilkinson. Guidance and activation of murine macrophages by nanometric scale topography. *Experimental Cell Research*, 1996. **223**(2): p. 426-435.

21. Wilkinson, C.D.W., A.S.G. Curtis, and J. Crossan. Nanofabrication in cellular engineering. *Journal of Vacuum Science & Technology B*, 1998. **16**(6): p. 3132-3136.

22. Poole-Warren, L.A., K. Schindhelm, A.R. Graham, P.R. Slowiaczek, and K.R. Noble. Performance of small diameter synthetic vascular prostheses with confluent autologous endothelial cell linings. *Journal of Biomedical Materials Research*, 1996. **30**(2): p. 221-229.

23. Dalton, B.A., G.A. McFarland, and J.G. Steele. Stimulation of epithelial tissue migration by certain porous topographies is independent of fluid flux. *Journal of Biomedical Materials Research*, 2001. **56**: p. 83-92.

24. Steele, J.G., G. Johnson, K.M. McLean, G.J. Beumer, and H.J. Griesser. Effect of porosity and surface hydrophilicity on migration of epithelial tissue over synthetic polymer. *Journal of Biomedical Materials Research*, 2000. **50**: p. 475-482.

25. Kirkpatrick, C.J., M. Otto, T.V. Kooten, V. Krump, J. Kriegsmann, and F. Bittinger. Endothelial cell cultures as a tool in biomaterial research. *Journal of Materials Science-Materials in Medicine*, 1999. **10**(10-11): p. 589-594.

26. Sato, M., K. Nagayama, N. Kataoka, M. Sasaki, and K. Hane. Local mechanical properties measured by atomic force microscopy for cultured bovine endothelial cells exposed to shear stress. *Journal of Biomechanics*, 2000. **33**: p. 127-135.

27. Tsukurov, O.I., C.J. Kwolek, G.J. L'Italien, A. Benbrahim, B.B. Milinazzo, N.E. Conroy, J.P. Gertler, R.W. Orkin, and W.M. Abbott. The Response of Adult Human Saphenous Vein Endothelial Cells to Combined Pressurized Pulsatile Flow and Cyclic Strain, In Vitro. *Annals of Vascular Surgery*, 2000. **14**: p. 260-267.

28. Vaidya, R., L.M. Tender, G. Bradley, M.J. O'Brien II, M. Cone, and G.P. Lopez. Computer-Controlled Laser Ablation: A Convenient and Versatile Tool for Micropatterning Biofunctional Synthetic Surfaces for Applications in Biosensing and Tissue Engineering. *Biotechnology Progress*, 1998. **14**: p. 371-377.

29. Kappelt, M. and D. Bimberg. Wet chemical etching of high quality V-grooves with {111} a sidewalls on (001) InP. *Journal of the Electrochemical Society*, 1996. **143**(10): p. 3271-3273.

30. Thomas, C.H., C.D. McFarland, M.L. Jenkins, A. Rezania, J.G. Steele, and K.E. Healy. The role of vitronectin in the attachment and spatial distribution of bone-derived cells on materials with patterned surface chemistry. *Journal of Biomedical Materials Research*, 1997. **37**(1): p. 81-93.

31. Tien, J., A. Terfort, and G.M. Whitesides. Microfabrication through Electrostatic Self-Assembly. *Langmuir*, 1997. **13**: p. 5349-5355.

32. Alaerts, J.A., V.M. De Cupere, S. Moser, P.V.B. de Aguilar, and P.G. Rouxhet. Surface characterization of poly(methyl methacrylate) microgrooved for contact guidance of mammalian cells. *Biomaterials*, 2001. **22**(12): p. 1635-1642.

33. Schmidt, J.A. and A.F. von Recum. Texturing of polymer surfaces at the cellular level. *Biomaterials*, 1991. **12**(4): p. 385-389.

34. von Recum, A.F. and T.G. van Kooten. The influence of micro-topography on cellular response and the implications for silicone implants. *Journal of Biomaterials Science - Polymer Edition*, 1995. **7**(2): p. 181-198.

35. Walboomers, X.F., W. Monaghan, A.S.G. Curtis, and J.A. Jansen. Attachment of fibroblasts on smooth and microgrooved polystyrene. *Journal of Biomedical Materials Research*, 1999. **46**: p. 212-220.

36. Matsuzaka, K., X.F. Walboomers, A. de Ruijter, and J.A. Jansen. Effect of microgrooved poly-l-lactic (PLA) surfaces on proliferation, cytoskeletal organization, and mineralized matrix formation of rat bone marrow cells. *Clinical Oral Implants Research*, 2000. **11**: p. 325-333.

37. den Braber, E.T., J.E. de Ruijter, L.A. Ginsel, A.F. von Recum, and J.A. Jansen. Orientation of ECM protein deposition, fibroblast cytoskeleton, and attachment complex components on silicone microgrooved surfaces. *Journal of Biomedical Materials Research*, 1998. **40**: p. 291-300.

38. den Braber, E.T., J.E. de Ruijter, H.T.J. Smits, L.A. Ginsel, A.F. von Recum, and J.A. Jansen. Quantitative analysis of cell proliferation and orientation on substrata with uniform parallel surface micro-grooves. *Biomaterials*, 1996. **17**(11): p. 1093-1099.

39. Walboomers, X.F., J.J.E. Croes, L.A. Ginsel, and J.A. Jansen. Growth behavior of fibroblasts on microgrooved polystyrene. *Biomaterials*, 1998. **19**: p. 1861-1868.

40. den Braber, E.T., J.E. de Ruijter, and J.A. Jansen. The effect of a subcutaneous silicone rubber implant with shallow surface microgrooves on the surrounding tissues in rabbits. *Journal of Biomedical Materials Research*, 1997. **37**: p. 539-547.

41. Walboomers, X.F. and J.A. Jansen. Microgrooved silicone subcutaneous implants in guinea pigs. *Biomaterials*, 2000. **21**: p. 629-636.

42. Walboomers, X.F., H.J.E. Croes, L.A. Ginsel, and J.A. Jansen. Microgrooved subcutaneous implants in the goat. *Journal of Biomedical Materials Research*, 1998. **42**: p. 634-641.

43. Dalton, B.A., X.F. Walboomers, M. Dziegielewski, M.D.M. Evans, S. Taylor, J.A. Jansen, and J.G. Steele. Modulation of epithelial tissue and cell migration by microgrooves. *Journal of Biomedical Materials Research*, 2001. **56**(2): p. 195-207.

44. Rich, A. and A.K. Harris. Anomalous preferences of cultured macrophages for hydrophobic and roughened substrata. *Journal of Cell Science*, 1981. **50**(Aug): p. 1-7.

45. Fujisawa, N., L.A. Poole-Warren, J.C. Woodard, C.D. Bertram, and K. Schindhelm. A novel textured surface for blood-contact. *Biomaterials*, 1999. **20**: p. 955-962.

46. Fujisawa, N., R.A. Odell, L.A. Poole-Warren, C.D. Bertram, J.C. Woodard, and K. Schindhelm. Acute cellular interaction with textured surfaces in blood contact. *Journal of Biomedical Materials Research*, 2000. **52**(3): p. 517-527.

47. Lincks, J., B.D. Boyan, C.R. Blanchard, C.H. Lohmann, Y. Liu, D.L. Cochran, D.D. Dean, and Z. Schwartz. Response of MG63 osteoblast-like cells to titanium and titanium alloy is dependent on surface roughness and composition. *Biomaterials*, 1998. **19**: p. 2219-2232.

48. Turner, A.M.P., N. Dowell, S.W.P. Turner, L. Kam, M. Isaacson, J.N. Turner, H.G. Craighead, and W. Shain. Attachment of astroglial cells to microfabricated pillar arrays of different geometries. *Journal of Biomedical Materials Research*, 2000. **51**: p. 430-441.

49. Tan, J., H. Shen, K.L. Carter, and W.M. Saltzman. Controlling human polymorphonuclear leukocytes motility using microfabrication technology. *Journal of Biomedical Materials Research*, 2000. **51**: p. 694-702.

50. Kaihara, S., J. Borenstein, R. Koka, S. Lalan, E.R. Ochoa, M. Ravens, H. Pien, B. Cunningham, and J.P. Vacanti. Silicon Micromachining to Tissue Engineer Branched Vascular Channels for Liver Fabrication. *Tissue Engineering*, 2000. **6**(2): p. 105-117.

51. Flemming, R.G., C.J. Murphy, G.A. Abrams, S.L. Goodman, and P.F. Nealey. Effects of synthetic micro- and nano-structured surfaces on cell behavior. *Biomaterials*, 1999. **20**: p. 573-588.

52. Carter, S.B. Haptotactic Islands - A Method of confining single cells to study individual cell reactions and clone formation. *Experimental Cell Research*, 1967. **48**(1): p. 189-.

53. Carter, S.B. Haptotaxis and mechanism of cell motility. *Nature*, 1967. **213**(5073): p. 256-.

54. Harris, A. Behavior of cultured cells on substrata of variable adhesiveness. *Experimental Cell Research*, 1973. **77**: p. 285-297.

55. Lopez, G.P., M.W. Albers, S.L. Schreiber, R. Carroll, E. Peralta, and G.M. Whitesides. Convenient Methods for Patterning the Adhesion of Mammalian Cells to Surfaces Using Self-Assembled Monolayers of Alkanethiolates on Gold. *Journal of the American Chemical Society*, 1993. **115**: p. 5877-5878.

56. Britland, S., P. Clark, P. Connolly, and G. Moores. Micropatterned Substratum Adhesiveness: A Model for Morphogenetic Cues Controlling Cell Behavior. *Experimental Cell Research*, 1992. **198**: p. 124-129.

57. McFarland, C.D., C.H. Thomas, C. DeFilippis, J.G. Steele, and K.E. Healy. Protein Adsorption and Cell Attachment to Patterned Surfaces. *Journal of Biomedical Materials Research*, 2000. **49**(2): p. 200-210.

58. Britland, S., H. Morgan, B. Wojiak-Stondart, M. Riehle, A. Curtis, and C. Wilkinson. Synergistic and Hierarchical Adhesive and Topographic Guidance of BHK cells. *Experimental Cell Research*, 1996. **228**: p. 313-325.

59. Folch, A. and M. Toner. Cellular Micropatterns on Biocompatible Materials. *Biotechnology Progress*, 1998. **14**: p. 388-392.

60. Kane, R.S., S. Takayama, E. Ostuni, D.E. Ingber, and G.M. Whitesides. Patterning proteins and cells using soft lithography. *Biomaterials*, 1999. **20**: p. 2363-2376.

61. Folch, A., B.-H. Jo, O. Hurtado, D.J. Beebe, and M. Toner. Microfabricated elastomeric stencils for micropatterning cell cultures. *Journal of Biomedical Materials Research*, 2000. **52**: p. 346-353.

62. Schmid, H. and B. Michel. Siloxane Polymers for High-Resolution, High-Accuracy Soft Lithography. *Macromolecules*, 2000. **33**: p. 3042-3049.

63. Kam, L. and S.G. Boxer. Cell adhesion to protein-micropatterned-supported lipid bilayer membranes. *Journal of Biomedical Materials Research*, 2001. **55**: p. 487-495.

64. Ostuni, E., C.S. Chen, D.E. Ingber, and G.M. Whitesides. Selective deposition of proteins and cells in arrays of microwells. *Langmuir*, 2001. **17**(9): p. 2828-2834.

65. Singhvi, R., A. Kumar, G.P. Lopez, G.N. Stephanopoulos, D.I.C. Wang, G.M. Whitesides, and D.E. Ingber. Engineering Cell Shape and Function. *Science*, 1994. **264**(5159): p. 696-698.

66. Chen, C.S., M. Mrksich, S. Huang, G.M. Whitesides, and D.E. Ingber. Micropatterned Surfaces for Control of Cell Shape, Position, and Function. *Biotechnology Progress*, 1998. **14**(3): p. 356-363.

67. Graham, L.M., D. Whittlesey, and B. Bevacqua. Cardiovascular Implantation, in *Biomaterials Science*, B.D. Ratner, A.S. Hoffman, F.J. Schoen, and J.E. Lemons, Editors. 1996, San Diego: Academic Press. p. 420-426.

68. Horbett, T.A. Proteins: Structure, Properties, and Adsorption to Surfaces, in *Biomaterials Science: An Introduction to Materials in Medicine*, B.D. Ratner, A.S. Hoffman, F.J. Schoen, and J.E. Lemons, Editors. 1996, San Diego, CA: Academic Press. p. 133-141.

69. Anderson, J.M. Inflammation, Wound Healing, and the Foreign Body Response, in *Biomaterials Science: An Introduction to Materials in Medicine*, B.D. Ratner, A.S. Hoffman, F.J. Schoen, and J.E. Lemons, Editors. 1996, San Diego, CA: Academic Press. p. 165-173.

70. Bartzoka, V., M.A. Brook, and M.R. McDermott. Protein-Silicone Interactions: How Compatible are the Two Species? *Langmuir*, 1998. **14**: p. 1887-1891.

71. Vroman, L., A.L. Adams, and M. Klings. Interactions among human blood proteins at interfaces. *Federation Proceedings*, 1971. **30**(5): p. 1494-.

72. Vroman, L., A.L. Adams, G.C. Fischer, and P.C. Munoz. Interaction of high molecular-weight kininogen, factor-XII, and fibrinogen in plasma at interfaces. *Blood*, 1980. **55**(1): p. 156-159.

73. Slack, S.M. and T.A. Horbett. The Vroman effect -- A critical review. *ACS Symposium Series-Proteins at Interfaces II*, 1995. **602**: p. 112-128.

74. Marieb, E. *Human Anatomy & Physiology*. 4 ed. 1998, Menlo Park: Benjamin/Cummings Science Publishing.

75. Seeley, R.R., T.D. Stephens, and P. Tate. *Anatomy & Physiology*. 4 ed. 1998, Boston: WCB/McGraw-Hill.

76. Bicknell, R. Introduction to the endothelial cell, in *Endothelial Cell Culture*, R. Bicknell, Editor. 1996, Cambridge: Cambridge University Press. p. 1-6.

77. Parikh, S.A. and E.R. Edelman. Endothelial cell delivery for cardiovascular therapy. *Advanced Drug Delivery Reviews*, 2000. **42**(1-2): p. 139-61.

78. Kochanek, K.D., B.L. Smith, and R.N. Anderson. *Deaths:Preliminary Data for 1999 - National vital statistics report*. 2001, Hyattsville, MD: National Center for Health Statistics, p. 49.

79. Veith, F.J., S.K. Gupta, E. Ascer, S. White-Flores, R.H. Samson, L.A. Scher, J.B. Towne, V.M. Bernhard, P. Bonier, W.R. Flinn, P. Astelford, J.S.T. Yao, and J.J. Bergan. Six year prospective multicenter randomized comparison of autologous saphenous vein and expanded polytetrafluoroethylene grafts in infrainguinal arterial reconstructions. *Journal of Vascular Surgery*, 1986. **3**: p. 104-114.

80. Dedisheim, P. and J.T. Watson. Cardiovascular Applications, in *Biomaterials Science: An Introduction to Materials in Medicine*, B.D. Ratner, A.S. Hoffman, F.J. Schoen, and J.E. Lemons, Editors. 1996, San Diego, CA: Academic Press. p. 283-297.

81. Graham, L.M., D. Whittlesey, and B. Bevacqua. Cardiovascular Implantation, in *Biomaterials Science: An Introduction to Materials in Medicine*, B.D. Ratner, A.S. Hoffman, F.J. Schoen, and J.E. Lemons, Editors. 1996, San Diego, CA: Academic Press. p. 420-426.

82. Bernex, F., J.P. Mazzucotelli, J.L. Roudiere, N. Benhaiem-Sigaux, J. Leandri, and D. Loisance. *In vitro* endothelialization of carbon-coated Dacron vascular grafts. *The International Journal of Artificial Organs*, 1992. **15**(3): p. 172-180.

83. Bhat, V.D., B. Klitzman, K. Koger, G.A. Truskey, and W.M. Reichert. Improving endothelial cell adhesion to vascular graft surfaces: Clinical need and strategies. *Journal of Biomaterials Science -- Polymer Edition*, 1998. **9**(11): p. 1117-1135.

84. Laube, H.R., J. Duwe, W. Rutsch, and W. Konertz. Clinical experience with autologous endothelial cell-seeded polytetrafluoroethylene coronary artery bypass grafts. *Journal of Thoracic and Cardiovascular Surgery*, 2000. **120**(1): p. 134-141.

85. Miwa, H., T. Matsuda, K. Kondo, N. Tani, Y. Fukaya, M. Morimoto, and F. Iida. Improved Patency of an Elastomeric Vascular Graft by Hybridization. *ASAIO Journal*, 1992. **38**(3): p. M512-M515.

86. Shinoka, T., D. Shum-Tim, P.X. Ma, R.E. Tanel, N. Isogai, R. Langer, J.P. Vacanti, and J. Mayer, J.E. Creation of Viable Pulmonary Artery Autografts Through Tissue Engineering. *Journal of Thoracic and Cardiovascular Surgery*, 1998. **115**(3): p. 536-545.

87. Balaban, N.Q., U.S. Schwarz, D. Riveline, P. Goichberg, G. Tzur, I. Sabanay, D. Mahalu, S. Safran, A. Bershadsky, L. Addadi, and B. Geiger. Force and focal adhesion assembly: a close relationship studied using elastic micropatterned substrates. *Nature Cell Biology*, 2001. **3**: p. 466-472.

88. Chandy, T., G.S. Das, R.F. Wilson, and G.H.R. Rao. Use of plasma glow for surface-engineering biomolecules to enhance bloodcompatibility of Dacron and PTFE vascular prosthesis. *Biomaterials*, 2000. **21**: p. 699-712.

89. Walpoth, B.H., R. Rogulenko, E. Tihvinskaia, S. Gogolewski, T. Schaffner, O.M. Hess, and U. Althaus. Improvement of patency rate in heparin-coated small synthetic vascular grafts. *Circulation*, 1998. **98**(19): p. Suppl: II319-23; discussion II324.

90. Patterson, R.B., A. Messier, and R.F. Valentini. Effects of Radiofrequency Glow Discharge and Oligopeptides on the Attachment of Human Endothelial Cells to Polyurethane. *ASAIO Journal*, 1995. **41**(3): p. M625-M629.

91. Ferrari, S. and B.D. Ratner. ToF-SIMS quantification of albumin adsorbed on plasma-deposited fluoropolymers by partial least-squares regression. *Surface and Interface Analysis*, 2000. **29**(12): p. 837-844.

92. Klee, D. and H. Hocker. Polymers for biomedical applications: Improvement of the interface compatibility, in *Advances in Polymer Science*. 1999. p. 1-57.

93. Qian, W.P., B. Xu, D.F. Yao, Y.H. Lin, L. Wu, C.X. Wang, F. Yu, Z.H. Lu, and Y. Wei. Site-directed immobilization of immunoglobulin G on 3-aminopropyltriethoxysilane modified silicon wafer surfaces. *Materials Science & Engineering C -- Biomimetic and Supramolecular Systems*, 1999. **8-9**: p. 475-480.

94. Hubbell, J.A., S.P. Massia, N.P. Desai, and P.D. Drumheller. Endothelial cell-selective materials for tissue engineering in the vascular graft via a new receptor. *Biotechnology*, 1991. **9**: p. 568-572.

95. Massia, S.P. and J.A. Hubbell. Vascular endothelial cell adhesion and spreading promoted by the peptide REDV of teh IIICS region of plasma fibronectin is mediated by integrin alpha 4 beta 1. *The Journal of Biological Chemistry*, 1992. **267**(20): p. 14019-14026.

96. Harris, A.K., P. Wild, and D. Stopak. Silicone Rubber Substrata: A New Wrinkle in the Study of Cell Locomotion. *Science*, 1980. **208**(4440): p. 177-179.

97. Lee, J., M. Leonard, T. Oliver, A. Ishihara, and K. Jacobson. Traction forces generated by locomoting keratocytes. *The Journal of Cell Biology*, 1994. **127**: p. 1957-1964.

98. Pelham, R.J. and Y.L. Wang. Cell Locomotion and Focal Adhesions are Regulated by Substrate Flexibility. *Proceedings of the National Academy of Sciences of the United States of America*, 1997. **94**(25): p. 13661-13665.

99. Dembo, M. and Y.L. Wang. Stresses at the cell-to-substrate interface during locomotion of fibroblasts. *Biophysical Journal*, 1999. **76**: p. 2307-2316.

100. Galbraith, C.G. and M.P. Sheetz. A micromachined device provides a new bend on fibroblast traction forces. *Proceedings of the National Academy of Sciences of the United States of America*, 1997. **94**: p. 9114-9118.

101. Chou, L., J.D. Firth, V.J. Uitto, and D.M. Brunette. Substratum surface topography alters cell shape and regulates fibronectin mRNA level, mRNA stability, secretion and assembly in human fibroblasts. *Journal of Cell Science*, 1995. **108**: p. 1563-1573.

102. Kato, S., J. Ando, and T. Matsuda. mRNA expression on shape-engineered endothelial cells: Adhesion molecules ICAM-1 and VCAM-1. *Journal of Biomedical Materials Research*, 2001. **54**: p. 366-372.

103. Chicurel, M.E., C.S. Chen, and D.E. Ingber. Cellular control lies in the balance of forces. *Current Opinion in Cell Biology*, 1998. **10**: p. 232-239.

104. Wang, J.H., E.S. Grood, J. Florer, and R. Wenstrup. Alignment and proliferation of MC3T3-E1 osteoblasts in microgrooved silicone substrata subjected to cyclic stretching. *Journal of Biomechanics*, 2000. **33**: p. 729-735.

105. Maniotis, A.J., C.S. Chen, and D.E. Ingber. Demonstration of mechanical connections between integrins, cytoskeletal filaments, and nucleoplasm that stabilize nuclear structure. *Proceedings of the National Academy of Sciences of the United States of America*, 1997. **94**: p. 849-854.

106. Arkles, B. Look what you can make out of silicones. *Chemtech*, 1983. **13**: p. 542-555.

107. Gerszten, P.C. A formal risk assessment of silicone breast implants. *Biomaterials*, 1999. **20**(11): p. 1063-1069.

108. Rosato, D.V. Polymers, processes and properties of medical plastics: including markets and applications, in *Biocompatible Polymers, Metals, and Composites*, M. Szycher, Editor. 1983, Lancaster, PA: Technomic Publ. p. 1019-1067.

109. Visser, S.A., R.W. Hergenrother, and S.L. Cooper. Polymers, in *Biomaterials Science: An Introduction to Materials in Medicine*, B.D. Ratner, A.S. Hoffman, F.J. Schoen, and J.E. Lemons, Editors. 1996, San Diego, CA: Academic Press. p. 50-60.

110. Quinn, K.J. and J.M. Courtney. Silicones as Biomaterials. *British Polymer Journal*, 1988. **20**: p. 25-32.

111. Widenhouse, C.W. Surface Modification of Vascular Prostheses and Intracorneal Lens Polymers [dissertation]. Gainesville: University of Florida; 1996.

112. Callow, M.E., J.A. Callow, J.D. Pickett-Heaps, and R. Wetherbee. Primary adhesion of Enteromorpha (Chlorophyta, Ulvales) propagules: Quantitative settlement studies and video microscopy. *Journal of Phycology*, 1997. **33**(6): p. 938-947.

113. Stanley, M.S., M.E. Callow, and J.A. Callow. Monoclonal antibodies to adhesive cell coat glycoproteins secreted by zoospores of the green alga *Enteromorpha*. *Planta*, 1999. **210**(1): p. 61-71.

114. Schultz, M.P., C.J. Kavanagh, and G.W. Swain. Hydrodynamic forces on barnacles: Implications on detachment from fouling-release surfaces. *Biofouling*, 1999. **13**(4): p. 323-335.

115. Swain, G.W., W.G. Nelson, and S. Preedeekanit. The influence of biofouling adhesion and biotic disturbance on the development of fouling communitites on non-toxic surfaces. *Biofouling*, 1998. **12**(1-3): p. 257-269.

116. Hillborg, H., M. Sandelin, and U.W. Gedde. Hydrophobic recovery of polydimethylsiloxane after exposure to partial discharges as a function of crosslink density. *Polymer*, 2001. **42**: p. 7349-7362.

117. Toth, A., I. Bertoti, M. Blazso, G. Banhegyi, A. Bognar, and P. Szaplonczay. Oxidative damage and recovery of silicone rubber surfaces. 1. X-ray photoelectron spectroscopic study. *Journal of Applied Polymer Science*, 1994. **52**(9): p. 1293-1307.

118. Zisman, W.A. Contact Angle: Wettability and Adhesion. 1964. Washington, D.C.: American Chemical Society.

119. Schmidt, J.A. and A.F. von Recum. Surface characterization of microtextured silicone. *Biomaterials*, 1992. **13**(10): p. 675-81.

120. Sperling, L.H. *Introduction to Physical Polymer Science*. 2 ed. 1992, New York: Wiley-Interscience. 594.

121. Mergerman, J., J.E. Hasson, D.F. Warnock, G.J. L'Italien, and W.M. Abbott. Noninvasive measurements of nonlinear arterial elasticity. *American Journal of Physiology*, 1986. **250**: p. H181-188.

122. Kendall, K. The adhesion and surface energy of elastic solids. *Journal of Physics D -- Applied Physics*, 1971. **4**(8): p. 1186-1195.

123. Good, R.J. Contact angle, wetting and adhesion: a critical review. *Journal of Adhesion Science and Technology*, 1992. **6**(12): p. 1269-1302.

124. *CRC handbook of chemistry and physics*. 78 ed. 1998, Cleveland, Ohio: CRC Press.

125. Johnson, R.E., Jr. and R.H. Dettre. Wettability and Contact Angles. *Surface and Colloid Science*, 1969. **2**: p. 85-153.

126. Patel, J.M., D.A. Edwards, E.R. Block, and M.K. Raizada. Effect of nitrogen dioxide on surface membrane fluidity and insulin receptor binding of pulmonary endothelial cells. *Biochem. Pharmacol.*, 1988. **37**(8): p. 1497-1507.

BIOGRAPHICAL SKETCH

Wade Richard Wilkerson was born on July 7, 1976, in Jacksonville, FL, to Dick and Nancy Wilkerson. He attended The Bolles School in Jacksonville where he received his high school diploma in 1994. In the Fall of 1994, Wade headed north to the University of Virginia, where he studied chemical engineering and received his Bachelor of Science degree in the Spring of 1998. His senior thesis involved the design of a testing apparatus for magnetic bearings in a vascular assist device. After graduating, Wade moved to Greenville, NC, and began work at Metrics, Inc. There he gained valuable experience in analytical chemistry and laboratory techniques under GLP and c-GMP guidelines. After one year in Greenville, Wade moved to Gainesville to begin his graduate work in Dr. Anthony Brennan's group as part of the Biomedical Engineering Program. During this time, he married Laura Holcomb on June 24, 2000. After graduation, Wade will begin a new phase of his education while studying to become a medical doctor at Wake Forest University Medical School in Winston-Salem, NC.